


**Härtlova, A., Erttmann, S.F., Raffi, F.A.M., Schmalz, A.M., Resch, U., Anugula, S., Lienenklaus, S., Nilsson, L.M., Kröger, A., Nilsson, J.A., Ek, T., Weiss, S., Gekara, N.O.**

**DNA Damage Primes the Type I Interferon System via the Cytosolic DNA Sensor STING to Promote Anti-Microbial Innate Immunity**

**(2015) Immunity, 42 (2), pp. 332-343.**

# DNA damage primes the type I interferon system via the cytosolic DNA sensor STING to promote anti-microbial innate immunity

Anetta Hartlova[1,2,3], Saskia F. Erttmann[1,2,3], Faizal AM. Raffi[1,2,3], Anja M. Schmalz[1,2,3], Ulrike Resch[1,2,3], Sharath Anugula[1,2,3], Stefan Lienenklaus[4], Lisa M. Nilsson[5], Andrea Kröger[4], Jonas A. Nilsson[5], Torben Ek[6], Siegfried Weiss[4] & Nelson O. Gekara[1,2,3]

[1]Laboratory for Molecular Infection Medicine Sweden,

[2]Department of Molecular Biology,

[3]Umeå Centre for Microbial Research

Umeå University, 90 187 Umeå, Sweden.

[4]Helmholtz Centre for Infection Research, 38124 Braunschweig, Germany

[5]Sahlgrenska Cancer Center, University of Gothenburg, 41390 Gothenburg

Gothenburg, Sweden

[6]Department of Paediatrics, Hospital of Halland, 30185 Halmstad, Sweden

**Correspondence** and requests for materials should be addressed to N.O.G. (Email: nelson.gekara@mims.umu.se)

## Running title: DNA damage primes the type I IFN system via STING

## Summary

Dysfunction in Ataxia-telangiectasia mutated (ATM), a central component of the DNA repair machinery, results in Ataxia Telangiectasia (AT), a cancer prone disease with a variety of inflammatory manifestations. By analyzing AT patient samples and *Atm*$^{-/-}$ mice, we found that unrepaired DNA lesions induce type I interferons (IFNs), resulting in enhanced anti-viral and anti-bacterial responses in *Atm*$^{-/-}$ mice. Priming of the type I interferon system by DNA damage involved release of DNA into the cytoplasm where it activated the STING pathway, which in turn enhanced responses to innate stimuli by activating the expression of Toll-like receptors, RIG-I-like receptors, cytoplasmic DNA sensors and their downstream signaling partners. This study provides a potential explanation for the inflammatory phenotype of AT patients and establishes damaged DNA as a cell intrinsic danger signal that primes the innate immune system for a rapid and amplified response to microbial and environmental threats.

## Introduction

Type I interferons (IFNs), the main effector cytokines against viral infections are induced mainly via the activation of pattern recognition receptors (PRRs) such as Toll-like receptors (TLRs), RIG-I-like receptors (RLRs) and the newly identified STING-dependent pathways that recognize microbial and self-DNA as well as cyclic dinucleotides in the cytoplasm (Kumar et al., 2011; Paludan and Bowie, 2013). While produced in large amounts during infections, it has long been acknowledged that type I IFNs are also produced spontaneously albeit at very low levels in the absence of infection (Lienenklaus et al., 2009). Such constitutively produced type I IFNs play a vital role in priming and maintaining the innate immune system in a "ready to go" state for prompt response upon microbial encounter (Hata et al., 2001; Taniguchi and Takaoka, 2001). Consequently, subtle changes in constitutive production of type I IFNs can have profound effects on the magnitude and quality of immune response elicited by microbes or other environmental danger signals (Gough et al., 2012; Hata et al., 2001; Taniguchi and Takaoka, 2001). Accordingly, if chronic, elevated constitutive type I IFNs may contribute to undesirable inflammatory responses and possibly autoimmunity (Arakura et al., 2007; Gough et al., 2012; Taniguchi and Takaoka, 2001). The molecular events underlying constitutive type I IFN induction and how defects in such events impact the onset and progression of disease remain unclear.

DNA damage is a constant threat to all eukaryotic life. DNA damage can be a result of exogenous genotoxic agents such as irradiation, UV light or chemical mutagens or due to endogenous genotoxic events such as DNA replication, recombination errors, metabolic genotoxins or oxidative stress. Of the various forms of damages inflicted by these mutagens, double-strand breaks (DSB) of DNA are the most toxic form. Ataxia-telangiectasia mutated (ATM) kinase plays a central role in double-strand DNA repair. In humans, loss of function

mutations in ATM results in Ataxia Telangiectasia (AT), a complex cancer prone neurodegenerative disease that displays a variety of inflammatory and autoimmune syndromes whose etiology remains unclear (Ammann and Hong, 1971; Deng et al., 2005; Kutukculer and Aksu, 2000; McGrath-Morrow et al., 2010; Shao et al., 2009; Westbrook and Schiestl, 2010). Furthermore, AT is associated with a peculiar susceptibility to respiratory bacterial infections (Boder and Sedgwick, 1958; Nowak-Wegrzyn et al., 2004; Schroeder and Zielen, 2013) and chronic herpesvirus infections (Kulinski et al., 2012; Masucci et al., 1984). Whereas such infections are presumed to be a result of defects in the adaptive immune system, curiously, severe systemic viral infections are disproportionately uncommon in such patients (Boder and Sedgwick, 1958; Nowak-Wegrzyn et al., 2004; Schroeder and Zielen, 2013). Whether ATM dysfunctions affect the innate immune system and whether that may contribute to AT associated features has not been addressed.

Here we show that accumulation of spontaneous DNA lesions in the absence of ATM or in response to exogenous genotoxic stress induces type I IFNs and that this primes the innate immune system for an amplified type I IFN response upon viral and bacterial encounter. We show that DNA damage induced type I IFN production is due to activation of STING pathway by self-DNA released into the cytoplasm.

## Results

### *Loss of ATM function results in a spontaneous type I interferon response*

While analyzing the role of ATM in innate immunity, we observed that sera from infection-free AT patients could protect HEK293 cells against the RNA virus, Vesicular stomatitis virus (VSV-GFP) (**Figure 1A, B**). The sera could activate expression of the interferon stimulated gene *Mx1* and nuclear factor-κ B (NF-κB) responses in HEK293 luciferase reporter cells (**Figure 1C, D**), indicating that ATM deficiency in human results in spontaneous systemic inflammation. We next analyzed fibroblasts from AT patients for the expression of type I IFN genes. Compared to those from apparently healthy subjects, AT patient fibroblasts had constitutively elevated transcripts for type I IFN genes *IFNB1* and *MX1* as well as for the type III IFN gene IFN-λ1 (*(IFNL1)* (**Figure 1E**). Upon infection with VSV-GFP, AT fibroblasts were found to elicit a higher IFNB1 response (**Figure 1F**) that correlated with diminished viral replication and progeny virus production (**Figure 1G, H**). Notably, silencing of IFNα and IFNβ receptor (IFNAR1) by shRNA rendered AT patient fibroblasts more permissive to VSV infection (**Figure 1I, J**) emphasizing the importance of type I IFNs in observed resistance of AT patient cells to VSV infection. To extend these findings, we also tested the responsiveness of AT patient cells to the DNA virus, type I herpes simplex virus (HSV1). Similarly, AT patient cells mounted a more robust IFNB1 response and resistance to HSV1 replication (**Figure 1K, L**). Together these results demonstrate that ATM dysfunction results in spontaneous type I IFN production which primes cells for an amplified anti-viral innate immune response.

To further study this phenomenon, we resorted to *Atm*$^{-/-}$ mice. Splenocytes (**Figure S1A**) and bone marrow derived macrophages (BMDMs) (**Figure S1B**) from *Atm*$^{-/-}$ mice showed constitutive elevation of *Ifnb1, Ifna4, Mx1* gene transcripts. Similarly, transcripts for the IFN-

inducible genes *Irf7* and *Sting (Tmem173)* - signaling molecules that are essential for an amplified type I IFN response (Honda et al., 2005; Ishikawa and Barber, 2008) were elevated in $Atm^{-/-}$ splenocytes and BMDMs at steady state.

***ATM deficiency primes the type I IFN system for enhanced anti-microbial response***

To better monitor the IFN induction *in vivo*, ATM-deficient mice were crossed with the sensitive IFN-β luciferase (Ifnb-luc) reporter mice (Lienenklaus et al., 2009). Whole body photo imaging revealed elevated systemic type I IFN response in $Atm^{-/-}Ifnb^{+/\Delta\beta\text{-}luc}$ mice at steady state as well as in response to VSV-AV2 (**Figure 2A**). VSV-AV2, a natural variant of VSV, is defective in its ability to inhibit anti-viral innate immunity and hence induces elevated type I IFNs (Stojdl et al., 2003). Accordingly, RT-PCR analysis revealed a stronger *Ifnb1* and *Mx1* response in $Atm^{-/-}$ BMDMs upon infection with VSV-AV2 (**Figure 2B**). Such an elevated type I IFN response coincided with inhibited replication and VSV-AV2 progeny production (**Figure 2C, D**). Further analysis of VSV RNA in splenocytes of mice infected with VSV-GFP also revealed inhibited *in vivo* replication of VSV in $Atm^{-/-}$ mice (**Figure 2E**). To verify these results, we employed lentiviral mediated shRNA silencing of *Atm* in the murine RAW 264.7 macrophage cell line. Compared to control shRNA macrophages, *Atm* silenced RAW 264.7 macrophages exhibited elevated *Ifnb1* transcript level at steady state (**Figure S2A, B**), recapitulating the situation observed in cells from AT patients or $Atm^{-/-}$ mice. In line, flow cytometric analysis revealed significantly inhibited replication of VSV-GFP in *Atm* silenced macrophages (**Figure S2C)**. Similarly, when infected with luciferase reporter HSV1 (HSV1-luc) strain (Summers and Leib, 2002), *Atm* silenced cells exhibited decreased HSV1 replication that coincided with enhanced *Ifnb1* response (**Figure S2D, E**). Together, these results indicate that loss of ATM results in a primed innate immune system which is more responsive and hence protective against viral infection.

Next we asked whether loss of ATM also primes cells for an amplified type I IFN induction in response to bacteria. *L. monocytogenes* is a facultative intracellular Gram-positive bacterium that triggers type I IFN response via multiple PRR pathways including TLRs as well as the cytoplasmic sensors for nucleic acids and cyclic dinucleotides (RLRs, CDRs) (Abdullah et al., 2012; Ishikawa et al., 2009; Woodward et al., 2010). *Atm*$^{-/-}$ BMDMs were found to elicit a higher IFN-β -luciferase response in response to *L. monocytogenes* infection (**Figure S2F**).

To elucidate which PRR pathways are primed by loss of ATM, BMDMs were stimulated with defined ligands for different PRRs including LPS (TLR4), $Pam_3CSK_4$ (TLR2), Poly(I:C) (TLR3) and Poly(dA:dT) (RLRs, CDRs). *Atm*$^{-/-}$ BMDMs elicited higher IFN-β -luciferase response to all such ligands (**Figure S2F)**, indicating that loss of ATM primes cells for an enhanced type I IFN induction in response to TLRs as well as cytoplasmic PRRs.

***ATM deficiency primes cells for enhanced activation of TBK1 upon viral or bacterial challenge***

TANK-binding kinase-1 (TBK1) is vital for activation of type I IFN response downstream of many PRRs. *Atm*$^{-/-}$ cells exhibited a higher and more sustained activation of TBK1 and p38 mitogen-activated protein kinase (p38 MAPK) upon *L. monocytogenes* infection (**Figure 3A, B**). Similarly, *Atm*$^{-/-}$ cells also exhibited elevated activation of the NF-κB pathway as judged by the faster rate of IkBα degradation (**Figure 3A**, **B**). Further ablation of the IFNα and β receptor (IFNAR1) in the *Atm*$^{-/-}$ background blunted the elevated proximal PRR signaling (**Figure 3A**, **B**) and *Ifnb1*, *Ifna4* and *Mx1* responses induced by *L. monocytogenes* (**Figure 3C**), demonstrating that amplified proximal PRR signaling and consequently type I IFN response in *Atm*$^{-/-}$ cells were due to the priming effect of spontaneously produced type I IFNs.

We also extended these analyses to VSV-AV2 infection. *Atm*$^{-/-}$ BMDMs exhibited elevated activation of proximal PRR signaling molecules including TBK1, p38 MAPK, and IRF3

(**Figure 3D**). Concomitantly, such cells displayed more a robust type I IFN response and hence an inhibited replication of VSV-AV2 (**Figure 3E, F**). Importantly, additional ablation of IFNAR in *Atm*$^{-/-}$ BMDMs resulted in more permissive replication of VSV-AV2 (**Figure E, 3F**). All together, these data show that loss of ATM results in a spontaneous production of type I IFNs which signal via IFNAR1 to prime cells for robust PRR mediated anti-microbial response.

***DNA damage primes the type I IFN system for an amplified IFN response upon microbial challenge***

To understand the mechanism underlying the amplified PRR signaling and type I IFN responses in *Atm*$^{-/-}$ cells, we asked whether elevated type I IFN production in *Atm*$^{-/-}$ cells was associated with the loss of DNA repair. We reasoned that if elevated type I IFN induction in *Atm*$^{-/-}$ cells was due to accumulation of unrepaired DNA lesions, then, induction of DNA damage in *Atm*$^{+/+}$ BMDM should recapitulate the type I IFN phenotype observed in *Atm*$^{-/-}$ cells. Indeed, exposure of wild type (Wt) BMDMs to γ-irradiation or the DNA damaging agent etoposide was found to induce *Ifnb1, Ifna4, Mx1, Irf7, Sting* (**Figure 4A)** as well as genes for several PRRs including *Tlr4, Tlr2, Rig-I*, the cytoplasmic DNA sensors cyclic GMP-AMP (cGAMP) synthase (MB21D1/cGAS) and *Ifi204* (human *IFI16*) (**Figure S3A-C)**. Upon further analysis, much like in *Atm*$^{-/-}$ cells, as shown above, Wt BMDMs exposed to DNA damage were found to be more responsive to the TLR ligands, LPS and $Pam_3CSK_4$, the STING agonist c-di-GMP (**Figure 4B)** or infection by *L. monocytogenes* or VSV-AV2 (**Figure 4C**). These results indicate that DNA damage induces the expression of various PRRs and downstream signaling partners such as IRF7 and STING, which together may contribute to priming the innate immune system for a rapid and amplified response upon microbial challenge.

***DNA damage primes the type I IFN system via STING***

TLRs, RLRs and CDRs are the main PRRs for type I IFN induction. Hence, we wanted to determine the specific PRR pathways involved in priming of the type I IFN system by DNA damage. To this end, we analyzed γ-irradiation-induced IFN-β luciferase response in BMDMs from *Ifnb*$^{+/\Delta\beta\text{-}luc}$ reporter mice deficient in the TLR adaptors MYD88 and TICAM1 (also known as TRIF) or the cytoplasmic DNA receptors STING. Whereas DNA damage could activate IFN-β luciferase responses in *Myd88*$^{-/-}$*Ifnb*$^{+/\Delta\beta\text{-}luc}$ and *Ticam1*$^{-/-}$ *Ifnb*$^{+/\Delta\beta\text{-}luc}$ BMDMs, such a response was abrogated in *Sting*$^{-/-}$*Ifnb*$^{+/\Delta\beta\text{-}luc}$ BMDMs (**Figure 5A**). *Myd88*$^{-/-}$, *Ticam1*$^{-/-}$ and *Sting*$^{-/-}$ BMDMs, however displayed wild type γ-H2A.X phophorylation upon γ-irradiation (**Figure 5B**), indicating that diminished type I IFN response in *Sting*$^{-/-}$ cells was not due to putative defects in DNA damage signaling. Next we asked whether ablation of the STING pathway affects DNA damage-induced priming of TLR signaling. In contrast to the *Ifnb*$^{+/\Delta\beta\text{-}luc}$, γ-irradiated *Sting*$^{-/-}$*Ifnb*$^{+/\Delta\beta\text{-}luc}$ BMDMs did not show a significantly enhanced IFN β luciferase response upon $Pam_3CSK_4$ or LPS stimulation (**Figure 5C)**. Thus, DNA damage primes the type I IFN system for enhanced TLR signaling via STING. Furthermore, similar to γ-irradiation, etoposide treatment also primed BMDMs for elevated IFN-β luciferase response (**Figure 5D)** and TBK1 activation (**Figure 5E)** by *L. monocytogenes* in a STING dependent manner. Much like in *Atm*$^{-/-}$ cells, priming of the type I IFN system by etoposide resulted in enhanced *Ifnb1* transcriptional response and inhibited replication of VSV (**Figure 5F, G)**. Similarly when challenged with HSV1, *Atm*$^{-/-}$ BMDMs or Wt BMDMs treated with etoposide mounted a higher *Ifnb1* transcriptional response and elevated TBK1 activation that coincided with suppressed HSV1 replication (**Figures S4A-D**).

Mice triply deficient in MYD88, TICAM1 and IPS-1 *(Myd88*$^{-/-}$*Ticam1*$^{-/-}$*Ips-1*$^{-/-}$*)* are defective in all major PRR pathways for type I IFN induction except the STING-dependent pathways. To specifically analyze STING-dependent priming of the type I IFN system by DNA damage,

*Myd88*$^{-/-}$*Ticam1*$^{-/-}$*Ips-1*$^{-/-}$ BMDMs were γ-irradiated and analyzed for type I IFN induction. Indeed, γ-irradiated *Myd88*$^{-/-}$*Ticam1*$^{-/-}$*Ips-1*$^{-/-}$ BMDMs also mounted a more robust *Ifnb1* and *Mx1* transcriptional response upon infection with *L. monocytogenes* (**Figure 5H**). Consistent with the type I IFN response, γ-irradiation alone was found to result in TBK1 activation in *Myd88*$^{-/-}$*Ticam1*$^{-/-}$*Ips-1*$^{-/-}$ BMDMs, which was further amplified upon *L. monocytogenes* infection (**Figure 5I**). Conversely, enhancement of TBK1 activation by γ-irradiation was abrogated in *Sting*$^{-/-}$ BMDMs (**Figure S4E**). Together, these observations indicate that DNA damage primes the innate immune system for robust anti-microbial response via the STING pathway.

***Loss of ATM primes the type I IFN system via STING pathway***

Next we sought to investigate whether the primed type I IFN state caused by loss of ATM was also dependent on the STING pathway. In this regard we ask whether ablation of ATM in the *Myd88*$^{-/-}$*Ticam1*$^{-/-}$*Ips-1*$^{-/-}$ background could also result in elevated type I IFN response at steady state as well as in response to infection. Therefore, we bred the *Myd88*$^{-/-}$*Ticam1*$^{-/-}$*Ips-1*$^{-/-}$ mice with *Atm*$^{-/-}$ animals. In comparison to those from *Myd88*$^{-/-}$*Ticam1*$^{-/-}$*Ips-1*$^{-/-}$ mice, peritoneal cells (PECs) from *Atm*$^{+/-}$*Myd88*$^{-/-}$*Ticam1*$^{-/-}$*Ips-1*$^{-/-}$ mice displayed higher *Ifnb1* and *Mx1* transcripts at steady state as well as in response to *L. monocytogenes* infection (**Figure 6A**). To unequivocally verify whether the primed type I IFN system caused by ATM deficiency was dependent on the STING pathway, we generated *Ifnb*$^{+/\Delta\beta\text{-}luc}$ mice deficient in ATM and STING (*Atm*$^{-/-}$*Sting*$^{-/-}$*Ifnb*$^{+/\Delta\beta\text{-}luc}$). Photo imaging of IFN-β luciferase activity of such mice and the corresponding BMDMs **(Figure 6B, D)** as well as *ex-vivo* analysis of *Ifnb1*, *Mx1*, *Irf7* and *Sting* transcripts in splenocytes from such mice **(Figure 6C)** revealed that ablation of the STING pathway could abrogate the elevated spontaneous type I IFN response caused by loss of ATM. cGAS (Wu et al., 2013) and IFI204 (human IFI16) (Jakobsen et al., 2013;

Unterholzner et al., 2010) are among the key DNA sensors upstream of STING. Similar to ablation of STING, knockdown of *cGas* and *Ifi204* by shRNA greatly decreased type I IFN response caused by ATM deficiency or the DNA damaging agent etoposide (**Figure 6E-H**). Thus, much like DNA damage, loss of ATM primes the type I IFN system via STING dependent mechanisms.

***DNA damage or loss of ATM releases ssDNA into cytoplasm thus activating the STING pathway***

Accumulation of DNA in the cytoplasm as a result of replication stress, DNA damage (Ahn et al., 2014; Yang et al., 2007) or replication intermediates of endogenous retroelements has previously been reported (Stetson et al., 2008). Therefore, to identify the endogenous molecules via which loss of ATM or DNA damage primes the type I IFN system, we analyzed cytoplasmic fractions for the presence of nucleic acids. Cytoplasmic extracts (CytExt) from *Atm*$^{-/-}$ BMDMs (*Atm*$^{-/-}$CytExt) or γ-irradiated Wt BMDMs (Wt/5Gy CytExt) were found to be enriched in nucleic acids. Upon further analysis, such CytExt DNA was found to be highly sensitive to ssDNA degrading enzyme S1 nuclease, but showed moderate sensitivity to DNase I which degrades dsDNA (**Figure 7A-C**). Thus, whereas a major fraction of DNA released into the cytoplasm upon DNA damage might be ssDNA, it appears that dsDNA also contributes. To study ssDNA in a more specific manner, we stained cytoplasm of Wt and *Atm*$^{-/-}$ BMDMs with anti-ssDNA antibody and analyzed by flow cytometry. *Atm*$^{-/-}$ BMDMs showed positive staining for ssDNA that was sensitive to S1 nuclease treatment (**Figure 7D**). Immunofluoresence microscopic analysis also confirmed accumulation of ssDNA in *Atm*$^{-/-}$ BMDMs as well as in fibroblasts from AT patients (**Figure 7E, F**).

Spontaneous accumulation of ssDNA and a concomitant *Ifnb1* induction was also evident in RAW 264.7 macrophages in which *Atm* was ablated by shRNA Atm (**Figure S5A-C**).

Remarkably, further silencing of *Sting* in such cells (shRNA Atm and Sting) abrogated elevated *Ifnb1* transcriptional response but not cytoplasmic ssDNA levels, indicating that diminished IFN response in cells doubly deficient in ATM and STING was due to defective recognition of cytoplasmic DNA and not DNA release into the cytoplasm (**Figure S5A, B**).

The exonuclease Trex1 is essential for clearance of DNA from the cytoplasm, hence its deficiency results in type I IFN driven autoimmunity syndromes (Crow and Rehwinkel, 2009; Gall et al., 2012; Stetson et al., 2008; Yang et al., 2007). In addition to a steady state expression, Trex1 has previously been shown to be induced by interferon-stimulatory DNA (Stetson et al., 2008). Consistently, *Trex1* transcripts were found upregulated in $Atm^{-/-}$ BMDMs and Atm shRNA silenced RAW 264.7 macrophages at steady state as well as in response to VSV infection in a STING dependent manner (**Figure S6A, D**), suggesting that *Trex1* is an inflammation inducible gene activated possibly to enable the cell cope with extraneous DNA in the cytoplasm. Thus, to further support the idea that the observed type I IFN phenotype was due to accumulation of DNA in cytoplasm of ATM deficient cells, we asked whether silencing of *Trex1* (shRNA Trex1) would augment the accumulation of cytoplasmic ssDNA and hence accentuate the spontaneous type I IFN response in *Atm* silenced cells (shRNA Atm). Indeed, ablation of *Trex1* in *Atm* silenced RAW 264.7 macrophages (shRNA Atm and Trex1) boosted accumulation of ssDNA in the cytoplasm (**Figure S6B**) and amplified spontaneous type I IFN response (**Figure S6C, D)**. To further explore, by quantitative PCR analysis, we evaluated if endogenous retroelements also accumulate in the cytoplasm of $Atm^{-/-}$ cells or upon DNA damage. Retrotransposon-like 1 (Rtl1) was found to be enriched in $Atm^{-/-}$ CytExt and Wt/5Gy CytExt (**Figure S6E**). Thus in addition to leakage from the nucleus, activation of endogenous retroelements may in part contribute to the observed accumulation of DNA in the cytoplasm upon DNA damage.

Triggering of cytoplasmic DNA receptors is associated with intracellular clustering of STING (Ahn et al., 2012; Ishikawa et al., 2009). In agreement with the above data, clustering of STING was discernible at steady state conditions in *Atm*$^{-/-}$ BMDMs as well as in Wt BMDMs treated with etoposide (**Figure 7G**). Upon transfection, *Atm*$^{-/-}$ CytExts but not Wt CytExts could induce STING clustering (**Figure 7G**) and activate IFN-β luciferase response in a STING dependent manner (**Figure 7H)**. Notably, consistent with an abundance of ssDNA, incubation with S1 nuclease effectively abrogated the type I IFN stimulatory activity of Wt/5Gy CytExt DNA. On the other hand DNase I had a moderate but significant effect, supporting the notion that dsDNA does also partially contribute to the observed responses (**Figure S7**). Together these results indicate that DNA damage results in release of DNA in the cytoplasm where it activates the STING pathway to prime the innate immune system.

## Discussion

Constitutive production of type I IFNs is vital for immune homeostasis and for maintaining the innate immune system stirred up for prompt response to microbial and other environmental danger signals. The cell intrinsic molecular events that trigger constitutive type I IFN production are unclear. In this study we show that DNA damage plays an important role in priming the type I IFN system. Consequently, DNA damage or loss of the DNA repair kinase ATM culminates in enhanced constitutive production of type I IFNs, elevated expression of different PRRs and their downstream signaling partners, which together may contribute to prime the innate immune system for a swift and amplified response upon microbial encounter.

Through crosses with a variety of mice defective in different PRR signaling pathways, we show that such priming is due to the activation of the STING pathway by DNA released into the cytoplasm upon DNA damage. A number of molecules including DAI, DHX9, DHX36, IFI204 (IFI16), DDX41, DXX60, Pol III, LRRFIP1, DNA-PK, and most recently cGAS (Wu et al., 2013) and the DNA repair protein Mre11(Kondo et al., 2013) have been proposed as direct cytoplasmic DNA sensors which act upstream of STING to induce type I IFNs (for review see Paludan SR and Bowie AG (Paludan and Bowie, 2013)). Our results indicate a role for cGAS and IFI204 in DNA damage mediated type I IFN induction. However, it is also conceivable that multiple receptors, most likely acting in a redundant and cell type specific manner, might contribute to the recognition of cytoplasmic DNA resulting from DNA lesions.

Activation of the type I IFN system by self-DNA has been linked to the etiology of variety of inflammatory diseases. Notably, accumulation of cytoplasmic ssDNA due to defects in the DNA exonuclease TREX1 (Stetson et al., 2008), or the 3’ exonuclease and deoxynucleotide (dNTP) triphosphohydrolase SAMHD1 (Behrendt et al., 2013; Tungler et al., 2013) has been

linked to Aicardi-Goutières syndrome (AGS). AGS is a neurodegenerative/inflammatory disease that mimics congenital viral infection and which phenotypically overlaps with the autoimmune disease systemic lupus erythematosus (Gall et al., 2012; Rice et al., 2007). Correspondingly, while stereotyped as a neurodegenerative disease, Ataxia Telangiectasia (AT), manifests a variety of inflammatory phenotypes including increased risk to cardiovascular diseases, type 2 diabetes, arthritis, colitis, multiple sclerosis and autoimmunity (Ammann and Hong, 1971; Deng et al., 2005; Kutukculer and Aksu, 2000; Meyts et al., 2003; Shao et al., 2009; Westbrook and Schiestl, 2010). Remarkably, the major cause of mortality and morbidity in AT patients is pulmonary insufficiency due to recurrent respiratory bacterial infections. Oddly, severe viral infections are uncommon in such patients. Recent clinical studies have shown that AT patients have systemic inflammation (McGrath-Morrow et al., 2010; Nowak-Wegrzyn et al., 2004; Schroeder and Zielen, 2013) and that anti-inflammatory medication rather than antibiotic treatment could suppress or even reverse lung deterioration in AT patients (Schroeder and Zielen, 2013). Clear-cut benefits of anti-inflammatory based therapy on progression of neurodegeneration in AT have also been reported (Giardino et al., 2013). Similarly, inhibition of ATM was recently shown to result in uncontrolled inflammatory response by glial cells, in turn driving neurodegeneration in drosophila (Petersen et al., 2012). Together, these increasing pieces of evidence buttress a hitherto underappreciated role of inflammation in the clinical manifestations of AT and proposes a mechanistic explanation for the disproportionate rarity of severe viral infections in such patients.

Finally and more broadly, the present findings establish a role of DNA damage in reviving up the innate immune system for enhanced anti-microbial innate immune responses. Consequently, tampering with DNA damage repair machinery, such as a kinase ATM, results in spontaneous production of type I IFNs which while priming the innate immune system for

a robust anti-viral defense might on the other hand contribute to unwarranted inflammation, much to the host´s detriment. Thus the type I IFN system under normal homeostatic conditions appears to be well balanced between priming and inflammation.

## Experimental Procedures

### Ethics statement

Experiments involving human subjects were done according to the recommendations of the local Research Ethics Committee of Umeå University (Regionala etikprövningsnämnden i Umeå) Sweden, as approved in permit Dnr 2012-501-31M. Fully informed consent was obtained from healthy and AT patients, in compliance with the Declaration of Helsinki. All mice were maintained under specific pathogen free conditions and experiments were approved and carried out according to the guidelines set out by the Regional Animal Ethic Committee Approval #A107-11 or A126-12.

### *In vivo* animal experiments

*In vivo* infection experiments were performed in Umeå Center for Comparative Biology (UCCB). An intraperitoneal (IP) dose of $10^5$ cfu was used for *L. monocytogenes* infection. An IP dose of 2 x $10^7$ pfu was used for VSV infections. Mice were anaesthetized using isoflurane in the XGI-8 gas anesthesia system (Caliper), injected with firefly luciferin then analyzed using the IVIS-200 system (Caliper). The software Living image 3.0 (Caliper) was used for image analysis and quantification of emission intensities.

### Cell Culture, viruses, stimulation, transfection and γ-irradiation

HEK293 cells, RAW 264.7 macrophages and human healthy (GM05294, Coriell Institute for Medical Research) and AT patient fibroblasts (GM02052, Coriell Institute for Medical Research) were maintained in DMEM containing 10 % (v/v) Fetal Calf Serum (FCS, Hyclone). Bone marrow-derived macrophages (BMDMs) were generated by culturing the mouse bone marrow cells in IMDM medium (Gibco, Life Technologies) supplemented with 10 % FCS (Gibco, Life Technologies), 100 U/ml penicillin (Sigma-Aldrich) and 100 g/ml streptomycin (Sigma-Aldrich), 2 mM glutamine (Sigma-Aldrich) and 20 % (v/v) L929 conditional medium. BMDMs were either stimulated with LPS (500 ng/ml), $Pam_3CSK_4$ (100

or 200 ng/ml), Poly(I:C) (30 μg/ml), c-di-GMP (20 μg/ml), *Listeria monocytogenes EGD-e* at a multiplicity of infection (MOI 20), VSV-GFP (Boritz et al., 1999) (MOI 1 or 10), VSV-AV2 (Stojdl et al., 2003) (MOI 1 or 10) or HSV type 1 strain KOS KOS/Dlux/OriL (HSV1-luc) (Summers and Leib, 2002) (MOI 0.1 or 1). Poly(dA:dT) (1 μg/ml) and isolated cytoplasmic DNA from WT, *Atm*$^{-/-}$ cells were transfected into macrophages using Lyovec according to manufacturer's instructions (Invivogen). BMDMs were γ-irradiated with a dose of 5Gy using Gammacell 40 irradiator (MDS Nordion).

**Immunofluorescence microscopy**

Cells cultured on coverslips were fixed with 4 % (w/v) paraformaldehyde in PBS for 15 min, permeabilized with 0.2 % (v/v) Triton-X100, blocked with 3 % (w/v) BSA in PBS for 30 min and then incubated with primary antibodies containing 1 % (w/v) BSA and 0.1 % (w/v) saponin in PBS for 1 h, washed with PBS then incubated with anti-rabbit IgG or anti-mouse IgM Alexa 488 fluorescence secondary antibodies for 1 h, respectively. Following washing, cells were stained with DAPI, washed with PBS and mounted onto microscope slides and imaged using a NIKON C1 confocal microscope.

**FACS analysis of ssDNA**

BMDMs were fixed in 80 % methanol in PBS, ±150 mM NaCl, without further treatment prior to adding antibody. Cells were pretreated with 200 U/ml S1 nuclease (Invitrogen) at 37 °C for 1 hr as indicated. FACS analysis of ssDNA-labeled cells were performed and analyzed by a Becton Dickinson *FACSCalibur* flow cytometer.

**Purification of Cytoplasmic DNA**

Cytoplasmic extract (CytExt) was isolated as previously described with minor modifications (Yang et al., 2007). Briefly, Wt, Wt + 5Gy γ-irradiated and *Atm*$^{-/-}$ BMDMs were lysed in 10 mM HEPES (pH 7.9), 10 mM KCl, 1.5 mM $MgCl_2$, 0.34 M sucrose, 10 % (v/v) glycerol,

plus protease inhibitors for 5 min on ice with 0.1 % (v/v) Triton X-100, and nuclei were removed by low-speed centrifugation (1500 x g, 10 min). Cytoplasmic protein extracts were treated with 1 mg/ml Proteinase K at 55 °C for 1 h. After phenol/chloroform extraction, the aqueous supernatant was incubated with 500 μg/ml DNase-free RNase A (QIAGEN) for 30 min at 37 °C, again followed by phenol/chloroform extraction. The DNA-containing aqueous phase was precipitated, resuspended in TE buffer, DNA concentrations were adjusted to the protein concentration of cytoplasmic fractions and analyzed by a 2 % (w/v) agarose gel in 1 x TBE buffer with 1 x GelRed stain (Biotium, Madison, WI) incorporated in gel.

**Statistical analysis**

All data are shown as mean ± S.E.M. Statistical analysis was performed using a two-tailed Student's *t-test* or analysis of variance (ANOVA) test followed by Bonferroni's post *hoc* test. For all tests, *P*-values less than 0.05 were considered statistically significant.

## Author Contributions

N.O.G conceived and designed the study, performed *in vivo* experiments. A.H, S.F.E, designed and performed experiment. F.A.M.R, U.R, A.M.S and S.A analyzed samples. S.L and S.W provided *Ifnb*$^{+/\Delta\beta\text{-}luc}$ mice. A.K, J.A.N and L.M.N contributed essential reagents. T.E was responsible for AT patients and contributed samples. A.H, S.F.E and N.O.G prepared the manuscript.

## Acknowledgement

This work was supported by funding from Laboratory for Molecular infection Medicine Sweden (MIMS). We are grateful to Dr. S. Akira, Osaka University, Japan, for Myd88$^{-/-}$, Ips-1-/- mice, Dr. DA Leib, Geisel School of Medicine at Dartmouth, USA, for HSV1 KOS KOS/Dlux/OriL strain (HSV1-luc). We thank Johanna Heine for technical assistance. This work was supported by Umeå University, Kempe foundation and Swedish Research Council grant 2011-2793 to N.O.G.

## References


Abdullah, Z., Schlee, M., Roth, S., Mraheil, M.A., Barchet, W., Bottcher, J., Hain, T., Geiger, S., Hayakawa, Y., Fritz, J.H., *et al.* (2012). RIG-I detects infection with live Listeria by sensing secreted bacterial nucleic acids. The EMBO journal *31*, 4153-4164.

Ahn, J., Gutman, D., Saijo, S., and Barber, G.N. (2012). STING manifests self DNA-dependent inflammatory disease. Proceedings of the National Academy of Sciences of the United States of America *109*, 19386-19391.

Ahn, J., Xia, T., Konno, H., Konno, K., Ruiz, P., and Barber, G.N. (2014). Inflammation-driven carcinogenesis is mediated through STING. Nature communications *5*, 5166.

Ammann, A.J., and Hong, R. (1971). Autoimmune phenomena in ataxia telangiectasia. The Journal of pediatrics *78*, 821-826.

Arakura, F., Hida, S., Ichikawa, E., Yajima, C., Nakajima, S., Saida, T., and Taki, S. (2007). Genetic control directed toward spontaneous IFN-alpha/IFN-beta responses and downstream IFN-gamma expression influences the pathogenesis of a murine psoriasis-like skin disease. Journal of immunology *179*, 3249-3257.

Behrendt, R., Schumann, T., Gerbaulet, A., Nguyen, L.A., Schubert, N., Alexopoulou, D., Berka, U., Lienenklaus, S., Peschke, K., Gibbert, K., *et al.* (2013). Mouse SAMHD1 has antiretroviral activity and suppresses a spontaneous cell-intrinsic antiviral response. Cell reports *4*, 689-696.

Boder, E., and Sedgwick, R.P. (1958). Ataxia-telangiectasia; a familial syndrome of progressive cerebellar ataxia, oculocutaneous telangiectasia and frequent pulmonary infection. Pediatrics *21*, 526-554.

Boritz, E., Gerlach, J., Johnson, J.E., and Rose, J.K. (1999). Replication-competent rhabdoviruses with human immunodeficiency virus type 1 coats and green fluorescent protein: entry by a pH-independent pathway. Journal of virology *73*, 6937-6945.

Crow, Y.J., and Rehwinkel, J. (2009). Aicardi-Goutieres syndrome and related phenotypes: linking nucleic acid metabolism with autoimmunity. Human molecular genetics *18*, R130-136.

Deng, X., Ljunggren-Rose, A., Maas, K., and Sriram, S. (2005). Defective ATM-p53-mediated apoptotic pathway in multiple sclerosis. Annals of neurology *58*, 577-584.

Gall, A., Treuting, P., Elkon, K.B., Loo, Y.M., Gale, M., Jr., Barber, G.N., and Stetson, D.B. (2012). Autoimmunity initiates in nonhematopoietic cells and progresses via lymphocytes in an interferon-dependent autoimmune disease. Immunity *36*, 120-131.

Giardino, G., Fusco, A., Romano, R., Gallo, V., Maio, F., Esposito, T., Palamaro, L., Parenti, G., Salerno, M.C., Vajro, P., and Pignata, C. (2013). Betamethasone therapy in ataxia telangiectasia: unraveling the rationale of this serendipitous observation on the basis of the pathogenesis. European journal of neurology : the official journal of the European Federation of Neurological Societies *20*, 740-747.

Gough, D.J., Messina, N.L., Clarke, C.J., Johnstone, R.W., and Levy, D.E. (2012). Constitutive type I interferon modulates homeostatic balance through tonic signaling. Immunity *36*, 166-174.

Hata, N., Sato, M., Takaoka, A., Asagiri, M., Tanaka, N., and Taniguchi, T. (2001). Constitutive IFN-alpha/beta signal for efficient IFN-alpha/beta gene induction by virus. Biochemical and biophysical research communications *285*, 518-525.

Honda, K., Yanai, H., Negishi, H., Asagiri, M., Sato, M., Mizutani, T., Shimada, N., Ohba, Y., Takaoka, A., Yoshida, N., and Taniguchi, T. (2005). IRF-7 is the master regulator of type-I interferon-dependent immune responses. Nature *434*, 772-777.

Ishikawa, H., and Barber, G.N. (2008). STING is an endoplasmic reticulum adaptor that facilitates innate immune signalling. Nature *455*, 674-678.

Ishikawa, H., Ma, Z., and Barber, G.N. (2009). STING regulates intracellular DNA-mediated, type I interferon-dependent innate immunity. Nature *461*, 788-792.

Jakobsen, M.R., Bak, R.O., Andersen, A., Berg, R.K., Jensen, S.B., Tengchuan, J., Laustsen, A., Hansen, K., Ostergaard, L., Fitzgerald, K.A., *et al.* (2013). IFI16 senses DNA forms of the lentiviral replication cycle and controls HIV-1 replication. Proceedings of the National Academy of Sciences of the United States of America *110*, E4571-4580.

Kondo, T., Kobayashi, J., Saitoh, T., Maruyama, K., Ishii, K.J., Barber, G.N., Komatsu, K., Akira, S., and Kawai, T. (2013). DNA damage sensor MRE11 recognizes cytosolic double-stranded DNA and induces type I interferon by regulating STING trafficking. Proceedings of the National Academy of Sciences of the United States of America *110*, 2969-2974.

Kulinski, J.M., Leonardo, S.M., Mounce, B.C., Malherbe, L., Gauld, S.B., and Tarakanova, V.L. (2012). Ataxia telangiectasia mutated kinase controls chronic gammaherpesvirus infection. Journal of virology *86*, 12826-12837.

Kumar, H., Kawai, T., and Akira, S. (2011). Pathogen recognition by the innate immune system. International reviews of immunology *30*, 16-34.

Kutukculer, N., and Aksu, G. (2000). Is there an association between autoimmune hemolytic anemia and ataxia-telangiectasia? Autoimmunity *32*, 145-147.

Lienenklaus, S., Cornitescu, M., Zietara, N., Lyszkiewicz, M., Gekara, N., Jablonska, J., Edenhofer, F., Rajewsky, K., Bruder, D., Hafner, M., *et al.* (2009). Novel reporter mouse reveals constitutive and inflammatory expression of IFN-beta in vivo. Journal of immunology *183*, 3229-3236.

Masucci, G., Berkel, I., Masucci, M.G., Ernberg, I., Szigeti, R., Ersoy, F., Sanal, O., Yegin, O., Henle, G., Henle, W., and et al. (1984). Epstein-Barr virus (EBV)-specific cell-mediated and humoral immune responses in ataxia-telangectasia patients. Journal of clinical immunology *4*, 369-382.

McGrath-Morrow, S.A., Collaco, J.M., Crawford, T.O., Carson, K.A., Lefton-Greif, M.A., Zeitlin, P., and Lederman, H.M. (2010). Elevated serum IL-8 levels in ataxia telangiectasia. The Journal of pediatrics *156*, 682-684 e681.

Meyts, I., Weemaes, C., De Wolf-Peeters, C., Proesmans, M., Renard, M., Uyttebroeck, A., and De Boeck, K. (2003). Unusual and severe disease course in a child with ataxia-telangiectasia. Pediatric allergy and immunology : official publication of the European Society of Pediatric Allergy and Immunology *14*, 330-333.

Nowak-Wegrzyn, A., Crawford, T.O., Winkelstein, J.A., Carson, K.A., and Lederman, H.M. (2004). Immunodeficiency and infections in ataxia-telangiectasia. The Journal of pediatrics *144*, 505-511.

Paludan, S.R., and Bowie, A.G. (2013). Immune sensing of DNA. Immunity *38*, 870-880.

Petersen, A.J., Rimkus, S.A., and Wassarman, D.A. (2012). ATM kinase inhibition in glial cells activates the innate immune response and causes neurodegeneration in Drosophila. Proceedings of the National Academy of Sciences of the United States of America *109*, E656-664.

Rice, G., Newman, W.G., Dean, J., Patrick, T., Parmar, R., Flintoff, K., Robins, P., Harvey, S., Hollis, T., O'Hara, A., *et al.* (2007). Heterozygous mutations in TREX1 cause familial chilblain lupus and dominant Aicardi-Goutieres syndrome. American journal of human genetics *80*, 811-815.

Schroeder, S.A., and Zielen, S. (2013). Infections of the respiratory system in patients with ataxia-telangiectasia. Pediatric pulmonology.

Shao, L., Fujii, H., Colmegna, I., Oishi, H., Goronzy, J.J., and Weyand, C.M. (2009). Deficiency of the DNA repair enzyme ATM in rheumatoid arthritis. The Journal of experimental medicine *206*, 1435-1449.

Stetson, D.B., Ko, J.S., Heidmann, T., and Medzhitov, R. (2008). Trex1 prevents cell-intrinsic initiation of autoimmunity. Cell *134*, 587-598.

Stojdl, D.F., Lichty, B.D., tenOever, B.R., Paterson, J.M., Power, A.T., Knowles, S., Marius, R., Reynard, J., Poliquin, L., Atkins, H., *et al.* (2003). VSV strains with defects in their ability to shutdown innate immunity are potent systemic anti-cancer agents. Cancer cell *4*, 263-275.

Summers, B.C., and Leib, D.A. (2002). Herpes simplex virus type 1 origins of DNA replication play no role in the regulation of flanking promoters. Journal of virology *76*, 7020-7029.

Taniguchi, T., and Takaoka, A. (2001). A weak signal for strong responses: interferon-alpha/beta revisited. Nature reviews. Molecular cell biology *2*, 378-386.

Tungler, V., Staroske, W., Kind, B., Dobrick, M., Kretschmer, S., Schmidt, F., Krug, C., Lorenz, M., Chara, O., Schwille, P., and Lee-Kirsch, M.A. (2013). Single-stranded nucleic acids promote SAMHD1 complex formation. Journal of molecular medicine *91*, 759-770.

Unterholzner, L., Keating, S.E., Baran, M., Horan, K.A., Jensen, S.B., Sharma, S., Sirois, C.M., Jin, T., Latz, E., Xiao, T.S., *et al.* (2010). IFI16 is an innate immune sensor for intracellular DNA. Nature immunology *11*, 997-1004.

Westbrook, A.M., and Schiestl, R.H. (2010). Atm-deficient mice exhibit increased sensitivity to dextran sulfate sodium-induced colitis characterized by elevated DNA damage and persistent immune activation. Cancer research *70*, 1875-1884.

Woodward, J.J., Iavarone, A.T., and Portnoy, D.A. (2010). c-di-AMP secreted by intracellular Listeria monocytogenes activates a host type I interferon response. Science *328*, 1703-1705.

Wu, J., Sun, L., Chen, X., Du, F., Shi, H., Chen, C., and Chen, Z.J. (2013). Cyclic GMP-AMP is an endogenous second messenger in innate immune signaling by cytosolic DNA. Science *339*, 826-830.

Yang, Y.G., Lindahl, T., and Barnes, D.E. (2007). Trex1 exonuclease degrades ssDNA to prevent chronic checkpoint activation and autoimmune disease. Cell *131*, 873-886.

## Figures

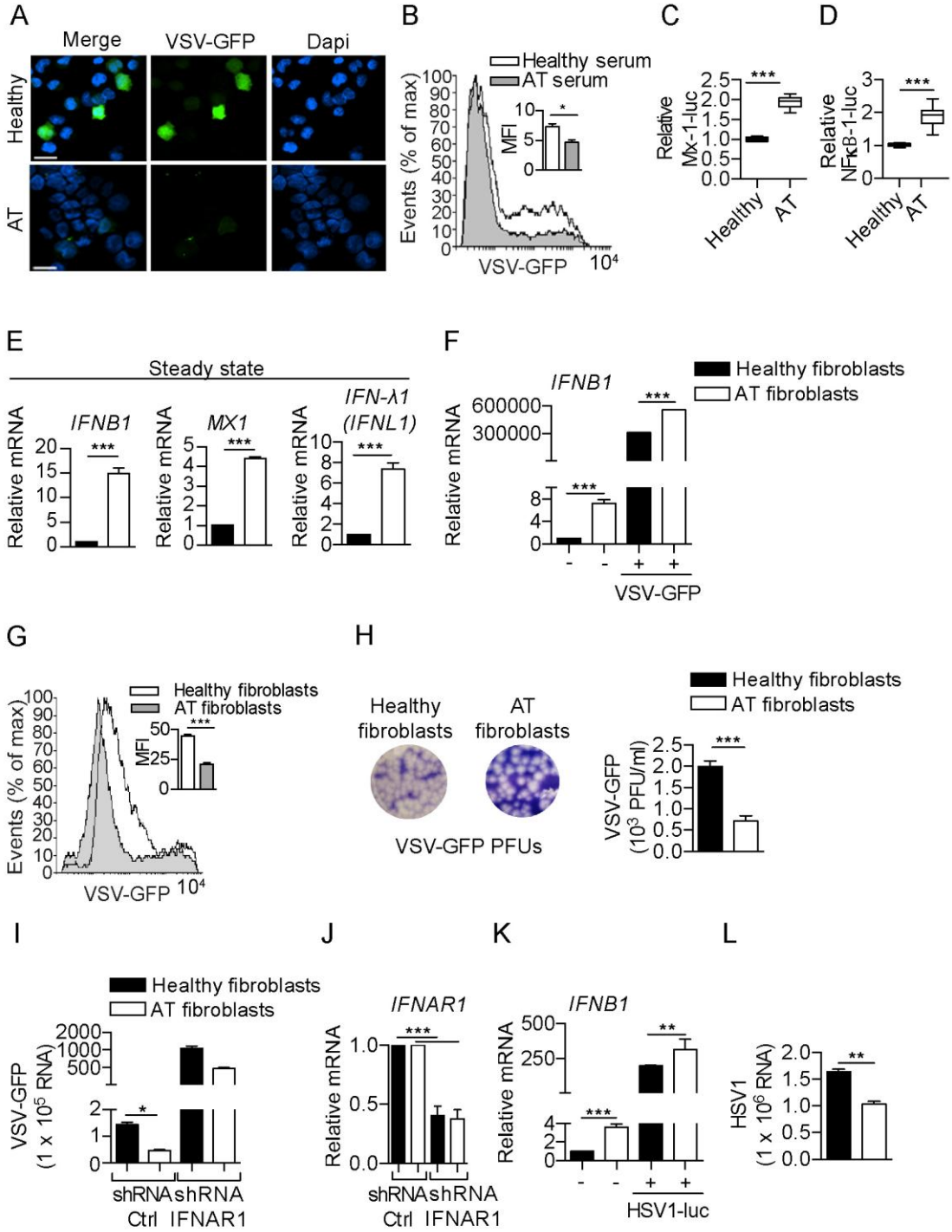


**Figure 1. ATM dysfunction in humans results in elevated spontaneous type I IFN response.** (**A** and **B)** Sera from AT patients protect against VSV infection. HEK293 cells pre-incubated for 12 hours with sera from apparently healthy subjects or AT patients infected with VSV-GFP (MOI 10), then analyzed for viral load by fluorescence microscopy (**A**) or flow cytometry (**B**) at 12 and 6 hours post infection, respectively. Insert in B depicts corresponding Median Fluorescence Intensity (MFI). (**C** and **D**) Sera from AT patients induce type I IFN and NF-κB activities in target cells. Luciferase activity in HEK293-Mx-1 (**C**) and HEK293-NF-κB (**D**) luciferase reporter cells incubated for 12 hours with sera from healthy subjects or AT patients (n=4). (**E**) qRT-PCR analysis of *IFNB1*, *IFNL1* and *MX1* mRNA in

healthy and AT fibroblasts at steady state. (**F**) qRT-PCR analysis of *IFNB1* in healthy and AT fibroblasts infected (or not) with VSV-GFP (MOI 10) for 6 hours. (**G**) Flow cytometric analysis of viral replication in healthy and AT fibroblasts infected with VSV-GFP for 6 hours. Insert depicts corresponding MFI. (**H**) Plaque assay of VSV-GFP titer in culture supernatants of healthy and AT fibroblasts 12 hours post infection. (**I**) qRT-PCR analysis of VSV-GFP RNA in healthy and AT fibroblasts transduced with control (Ctrl) shRNA or *IFNAR1* shRNA then infected with VSV-GFP for 6 hours. (**J**) Efficiency of *IFNAR1* knockdown in human healthy and AT fibroblasts analyzed by qRT-PCR. (**K**) qRT-PCR analysis of *IFNB1* in healthy and AT fibroblasts infected with HSV1-luciferase (HSV1-luc) (MOI 1) for 6 hours. (**L**) qRT-PCR estimation of HSV1 replication (RNA) in healthy and AT patients fibroblasts infected with HSV1-luc for 6 hours. Results are representative of two to three independent experiments. Data are shown as mean ± SEM. ***$P < 0.001$; (Student's *t*-test or one-way ANOVA followed by Bonferroni's post-test).

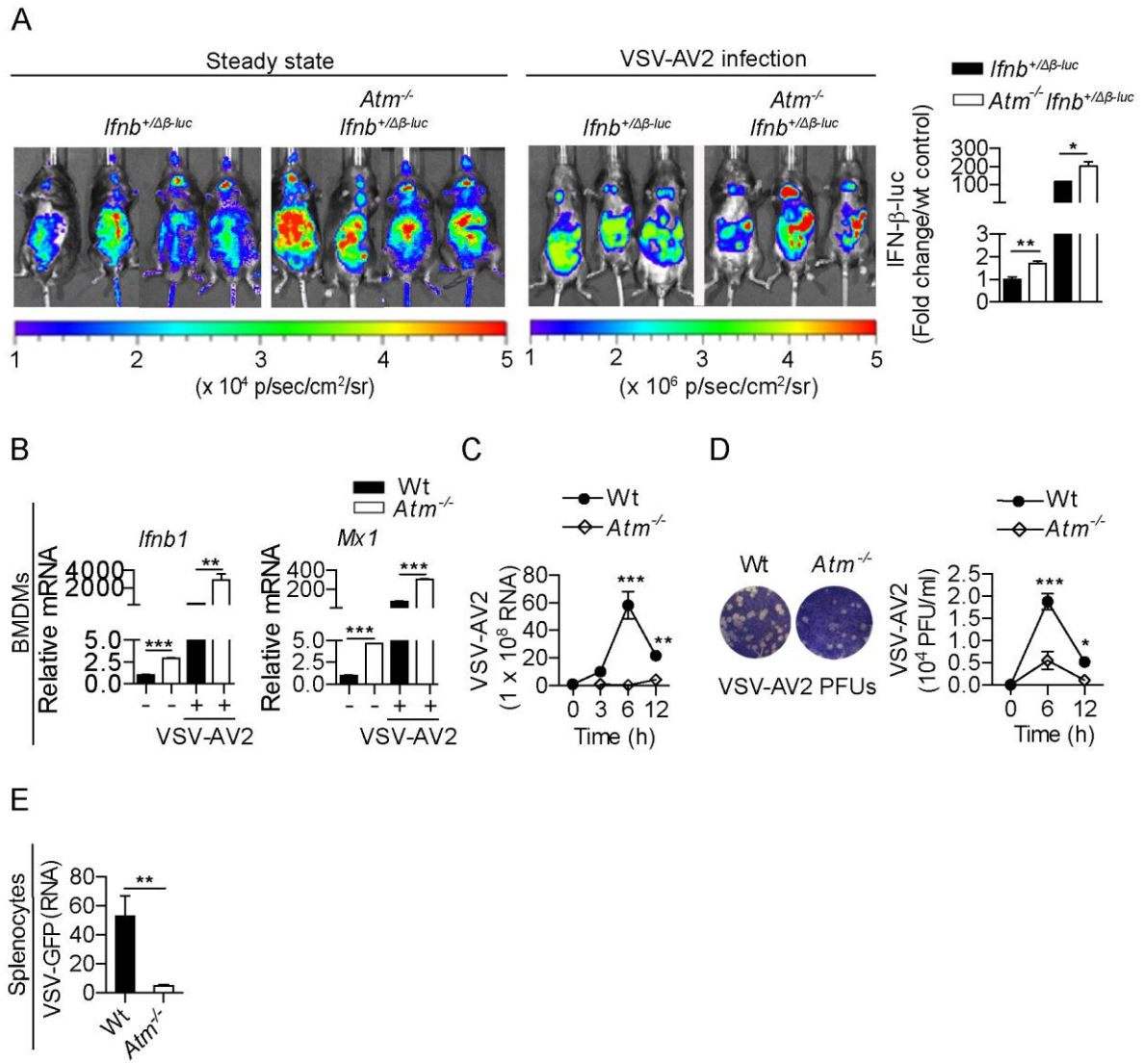


**Figure 2. Loss of *ATM primes the type I IFN system for an enhanced antiviral innate immunity.* (A)** Bioluminescence imaging of IFN-β luciferase response in representative pairs of *Ifnb*$^{+/\Delta\text{-luc}}$ or *Atm*$^{-/-}$*Ifnb*$^{+/\Delta\beta\text{-luc}}$ mice at steady state and 6 hours post intraperitoneal infection with VSV-AV2 (2 x $10^7$ pfu/mouse). The rainbow scale indicates the number of photons measured per second per $cm^2$ per steradian (sr). Quantification of fold change in IFN-β luciferase activity of *Atm*$^{-/-}$*Ifnb*$^{+/\Delta\beta\text{-luc}}$ mice in panel **A** compared to *Ifnb*$^{+/\Delta\beta\text{-luc}}$. (**B**) qRT-PCR analysis of *Ifnb1* and *Mx1* mRNA in Wt or *Atm*$^{-/-}$ BMDMs 6 hours post infection (or not) with VSV-AV2 (MOI 1). **(C** and **D)** qRT-PCR analysis of VSV RNA (**C**) and plaque forming assay in (**D**) BMDMs infected with VSV-AV2 (MOI 1) for the indicated time points. (**E**) qRT-PCR analysis of VSV RNA in splenocytes of Wt or *Atm*$^{-/-}$ mice 24 hours post infection with VSV-GFP. Results are representative of two to four independent experiments. Data are shown as mean ± SEM. **P*< 0.05, ***P*< 0.01, ****P*< 0.001; (Student's *t*-test or one-way ANOVA followed by Bonferroni's post-test). Also see **Figures S1 – S2.**

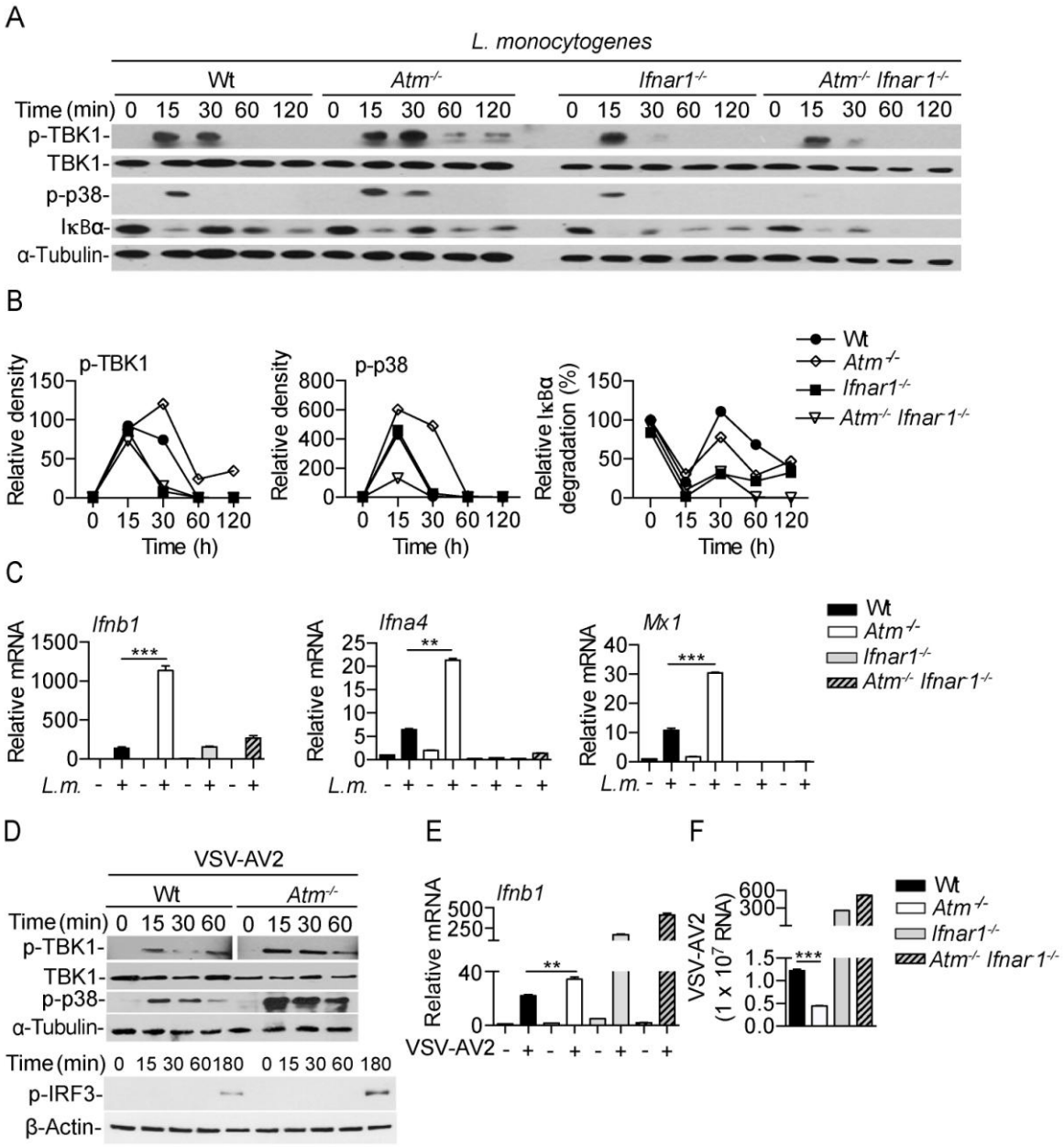


**Figure 3. Loss of ATM primes cells for enhanced TBK1 activation and type I IFN induction via IFNAR1**. (**A** and **B)** Immunoblots (**A**) of p-TBK1, total TBK1, p-P38 MAPK, IκBα in Wt, *Atm*$^{-/-}$, *Ifnar1*$^{-/-}$ and *Atm*$^{-/-}$*Ifnar1*$^{-/-}$ BMDMs infected with *L. monocyogenes* (*L.m.)* (MOI 20) for the indicated time points. (**B**) Quantification of immunoblots in **A** normalized to α-Tubulin and presented as relative densities (pTBK1, p-p38) or percentage of IκBα degradation compared to Wt control. (**C**) qRT-PCR analysis of *Ifnb1*, *Ifna4* and *Mx1* mRNA in Wt, *Atm*$^{-/-}$, *Ifnar1*$^{-/-}$ and *Atm*$^{-/-}$*Ifnar1*$^{-/-}$ BMDMs infected with *L.m.* for 6 hours. (**D)** Immunoblot analysis of p-TBK1, total TBK1, p-p38 MAPK and p-IRF3 in Wt, and *Atm*$^{-/-}$ BMDMs infected with VSV-AV2 (MOI 10) for the indicated time points. (**E**) qRT-PCR analysis of *Ifnb1* mRNA in Wt, *Atm*$^{-/-}$, *Ifnar1*$^{-/-}$, and *Atm*$^{-/-}$*Ifnar1*$^{-/-}$ BMDMs infected with VSV-AV2 (MOI 1) for 12 hours. (**F**) qRT-PCR analysis of viral RNA in BMDMs infected with VSV-AV2 for 12 hours. Results are representative of three independent experiments. Data are shown as mean ± SEM. ** *P*< 0.01, ***$P$< 0.001; (One-way ANOVA followed by Bonferroni's post-test).

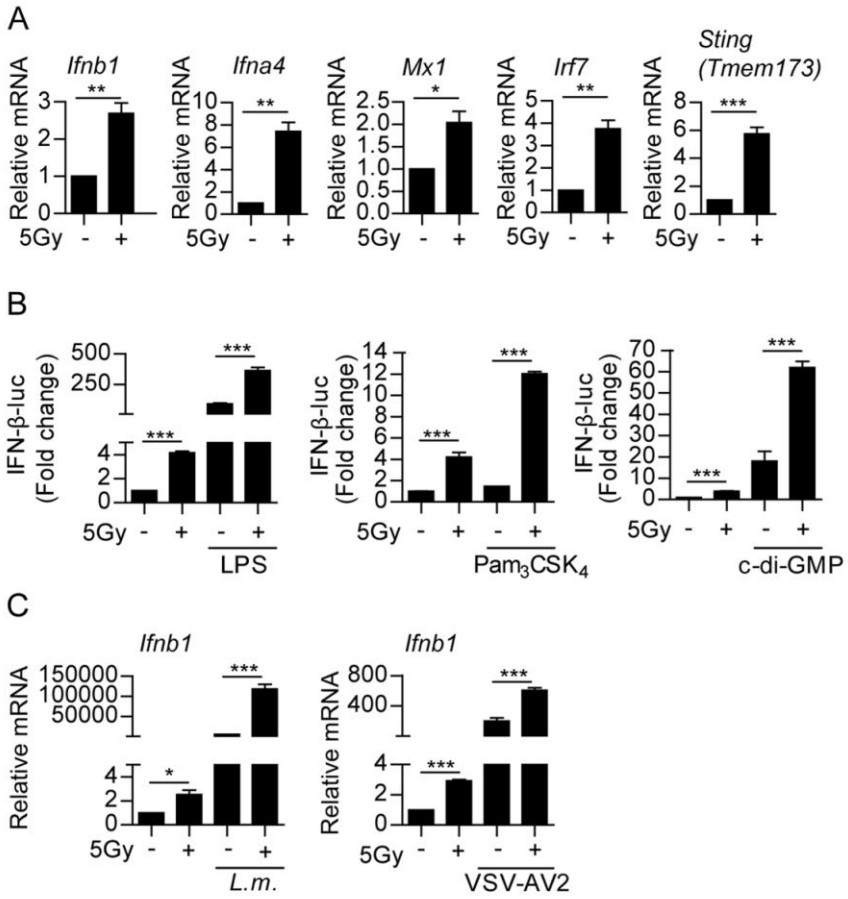


**Figure 4. DNA damage primes the type I IFN system for an enhanced induction of type I IFNs. (A)** qRT-PCR analysis of *Ifnb1*, *Ifna4*, *Mx1*, *Irf7* and *Sting* mRNA in Wt BMDMs 6 hours after γ-irradiation (5Gy). (**B)** Luciferase activity in *Ifnb*$^{+/\Delta\beta\text{-luc}}$ BMDMs primed (or not) by γ-irradiation (5Gy) as in **(A**) and then stimulated with LPS (500 ng/ml), $Pam_3CSK_4$ (100 ng/ml) or stimulated with c-di-GMP (20 μg/ml) for 6 hours. (**C**) qRT-PCR analysis of *Ifnb1* mRNA in Wt BMDMs that were primed (or not) by γ-irradiation as in (**A**) and then infected with *L.m.* (MOI 20) or VSV-AV2 (MOI 1) for 6 hours. Results are representative of three independent experiments. Data are shown as mean ± SEM. **P*< 0.05, ***P*< 0.01, ****P*< 0.001; (Student's *t*-test). Also see **Figure S3**.

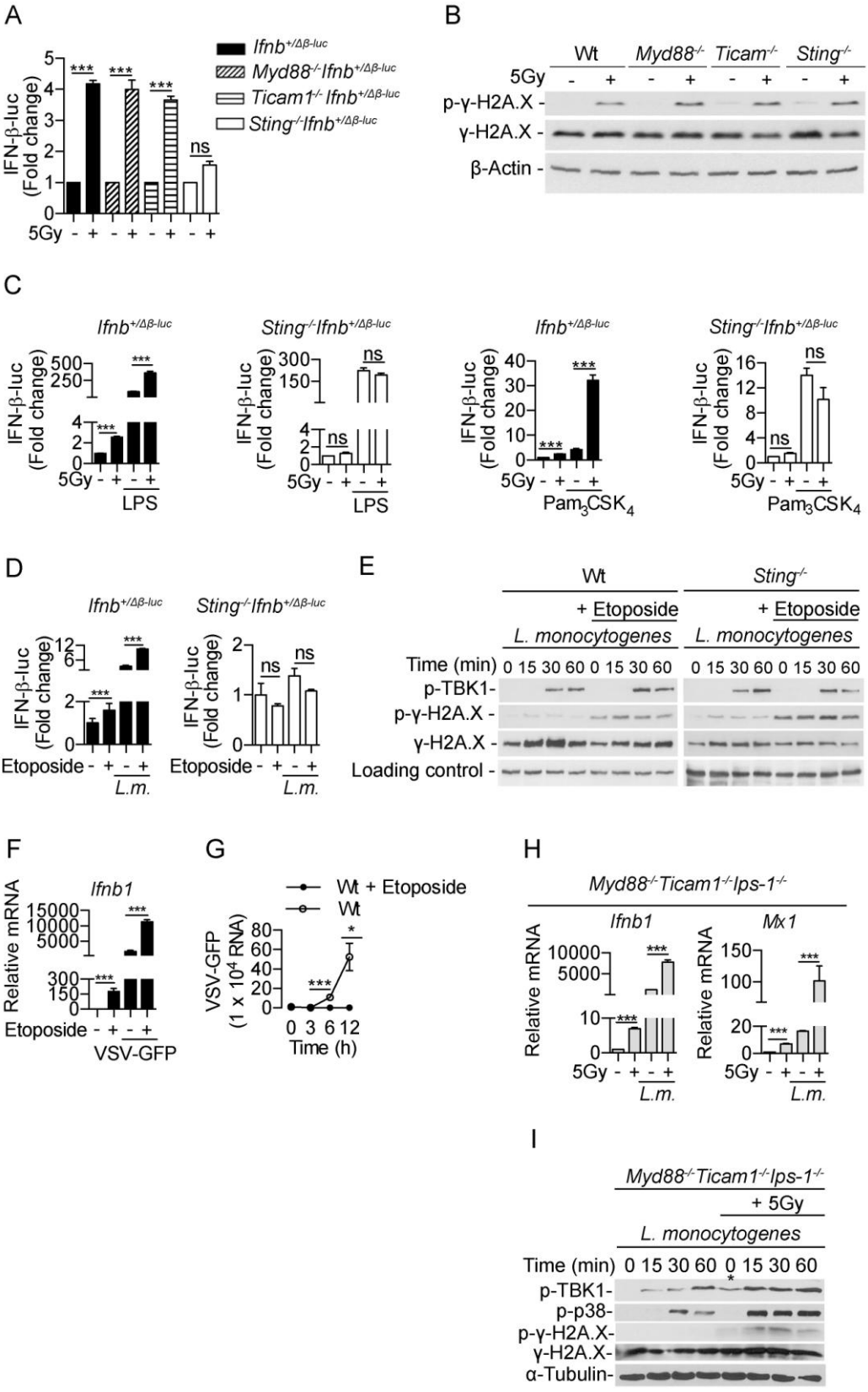


**Figure 5. DNA damage primes the type I IFN system via STING.** (**A**) IFN-β luciferase response in *Ifnb*$^{+/\Delta\beta\text{-luc}}$, *Myd88*$^{-/-}$*Ifnb*$^{+/\Delta\beta\text{-luc}}$, *Ticam1*$^{-/-}$*Ifnb*$^{+/\Delta\beta\text{-luc}}$, *Sting*$^{-/-}$*Ifnb*$^{+/\Delta\beta\text{-luc}}$ BMDMs 6 hours after γ-irradiation. (**B)** Immunoblot analysis of γ-H2A.X phosphorylation in Wt, *Myd88*$^{-/-}$, *Ticam1*$^{-/-}$ *and Sting*$^{-/-}$ BMDMs 1 hours after γ-irradiation. (**C**) IFN-β luciferase

response in *Ifnb*$^{+/\Delta\beta\text{-}luc}$, *Sting*$^{-/-}$*Ifnb*$^{+/\Delta\beta\text{-}luc}$ BMDMs primed (or not) by γ-irradiation for 6 hours and then stimulated with LPS (500 ng/ml) or $Pam_3CSK_4$ (100 ng/ml) for 6 hours. (**D**) IFN-β luciferase response in *Ifnb*$^{+/\Delta\beta\text{-}luc}$, *Sting*$^{-/-}$*Ifnb*$^{+/\Delta\beta\text{-}luc}$ BMDMs pre-treated (or not) with etoposide (50 μM) for 18 hours and then infected with *L.m.* (MOI 20) for 3 hours. (**E**) Immunoblot analysis of p-TBK1, p-γ-H2A.X and total γ-H2A.X in BMDMs pre-treated (or not) with etoposide (50 μM) for 18 hours and then infected with *L.m.* (MOI 20) for the indicated time points. (**F** and **G**), qRT-PCR analysis of *Ifnb1* (**F**) and VSV RNA (**G**) in BMDMs pre-treated (or not) with etoposide (50 μM) for 18 hours and then infected with VSV-GFP for 3 hours or the indicated time points. (**H**) qRT-PCR analysis of *Ifnb1* and *Mx1* mRNA in *Myd88*$^{-/-}$*Ticam1*$^{-/-}$*Ips-1*$^{-/-}$ BMDMs primed (or not) by γ-irradiation (5Gy) and infected with *L.m.* (MOI 20) for 6 hours. (**I**) Immunoblot analysis of p-TBK1, p-p38 MAPK and p-γ-H2A.X in *Myd88*$^{-/-}$*Ticam1*$^{-/-}$*Ips-1*$^{-/-}$ BMDMs γ-irradiated (or not) and then infected with *L.m.* (MOI 20) for the indicated time points. * highlights basal phosphorylation of TBK1 upon γ-irradiation. Results are representative of two to three independent experiments. Data are shown as mean ± SEM. **P*< 0.05, ***P*< 0.01, ****P*< 0.001; (one-way ANOVA followed by Bonferroni post-test or Student's *t*-test). Also see **Figure S4.**

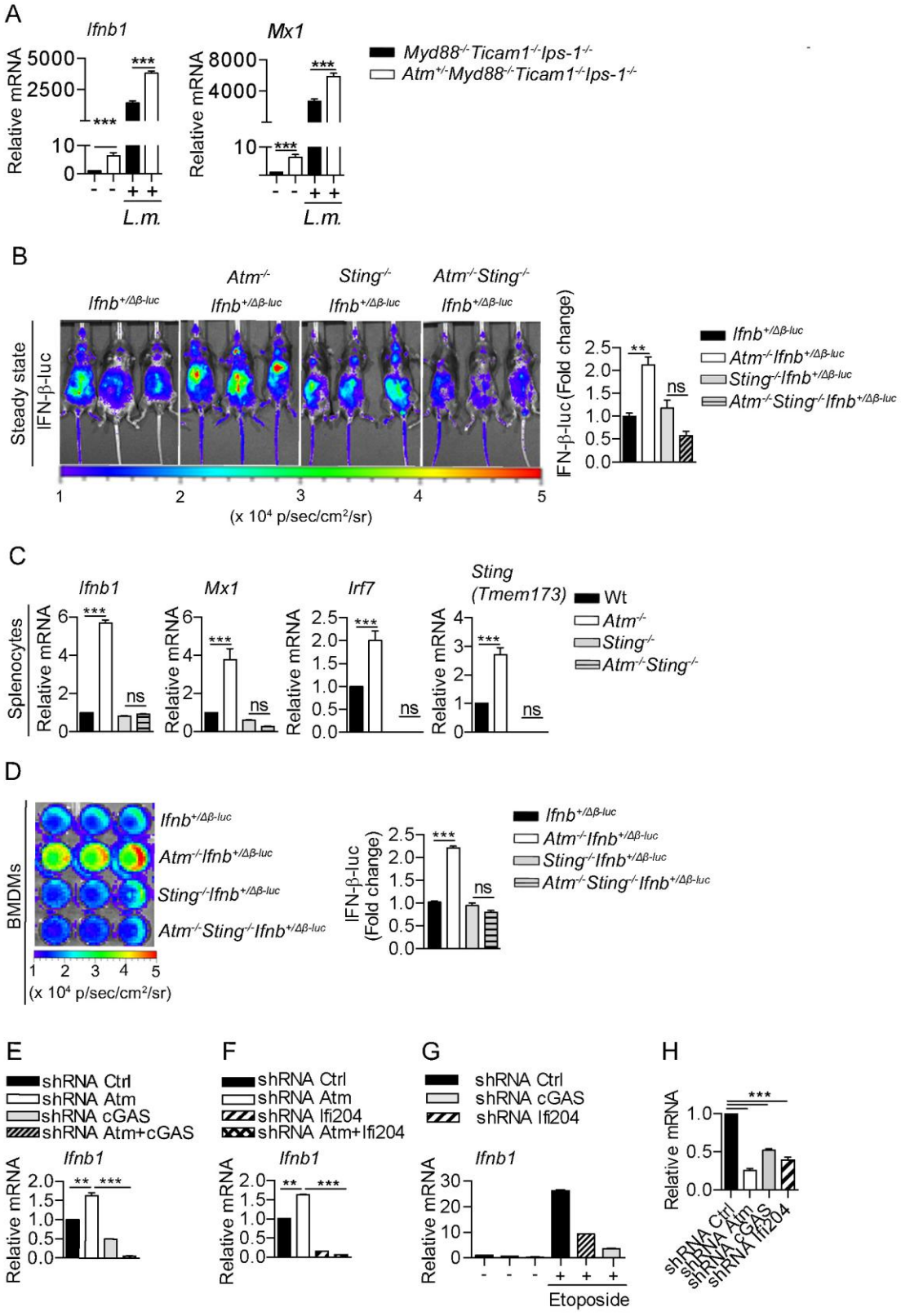


**Figure 6. Loss of ATM primes the type I IFN system via STING. (A)** qRT-PCR analysis of *Ifnb1* and *Mx1* in peritoneal cells isolated from *Myd88*$^{-/-}$*Ticam1*$^{-/-}$*Ips-1*$^{-/-}$ and *Atm*$^{+/-}$*Myd88*$^{-/-}$ *Ticam1*$^{-/-}$ *Ips-1*$^{-/-}$ mice infected (or not) with *L.m.* ($10^5$ cfu /mouse) for 6 hours. (**B**) *In vivo* photo imaging and corresponding spontaneous IFN-β luciferase activities in *Ifnb*$^{+/\Delta\beta\text{-luc}}$, *Atm*$^{-/-}$ *Ifnb*$^{+/\Delta\beta\text{-luc}}$, *Sting*$^{-/-}$*Ifnb*$^{+/\Delta\beta\text{-luc}}$, *Atm*$^{-/-}$*Sting*$^{-/-}$*Ifnb*$^{+/\Delta\beta\text{-luc}}$ mice. Luciferase expression is represented by a color shift from blue to red. Graph depicts corresponding fold change in

IFN-β luciferase activity relative to *Ifnb*$^{+/\Delta\beta\text{-}luc}$. (**C)** qRT-PCR analysis of *Ifnb*, *Mx1*, *Irf7* and *Sting* mRNA in splenocytes from Wt, *Atm*$^{-/-}$, *Sting*$^{-/-}$ and *Atm*$^{-/-}$*Sting*$^{-/-}$ mice at steady state. (**D)** Photo imaging of spontaneous IFN-β-luc response in BMDMs from *Ifnb*$^{+/\Delta\beta\text{-}luc}$, *Atm*$^{-/-}$*Ifnb*$^{+/\Delta\beta\text{-}luc}$, *Sting*$^{-/-}$*Ifnb*$^{+/\Delta\beta\text{-}luc}$ and *Atm*$^{-/-}$*Sting*$^{-/-}$*Ifnb*$^{+/\Delta\beta\text{-}luc}$ mice. Graph depicts corresponding fold change in IFN-β luciferase activities relative to Wt BMDMs. (**E**) qRT-PCR analysis of *Ifnb1* mRNA in RAW 264.7 macrophages silenced by shRNA for *Atm, cGas* or both (shRNA Atm + cGAS). (**F**) qRT-PCR analysis of *Ifnb1* mRNA in RAW 264.7 macrophages shRNA silenced for *Atm, Ifi204* or both (shRNA Atm + Ifi204). **(G**) qRT-PCR analysis of *Ifnb1* mRNA in RAW 264.7 macrophages silenced by shRNA for *cGAS* or *Ifi204* then stimulated (or not) with etoposide (50 µM) for 18 hours. (**H**) shRNA knockdown efficiency of *Atm, cGAS* and *Ifi204* in silenced RAW macrophages used in **E**-**F**, as revealed by qRT-PCR. Results are representative of two to three independent experiments. Data are shown as mean ± SEM. ***P*< 0.01, ****P*< 0.001; (one-way ANOVA followed by Bonferroni's post-test or Student's *t*-test).

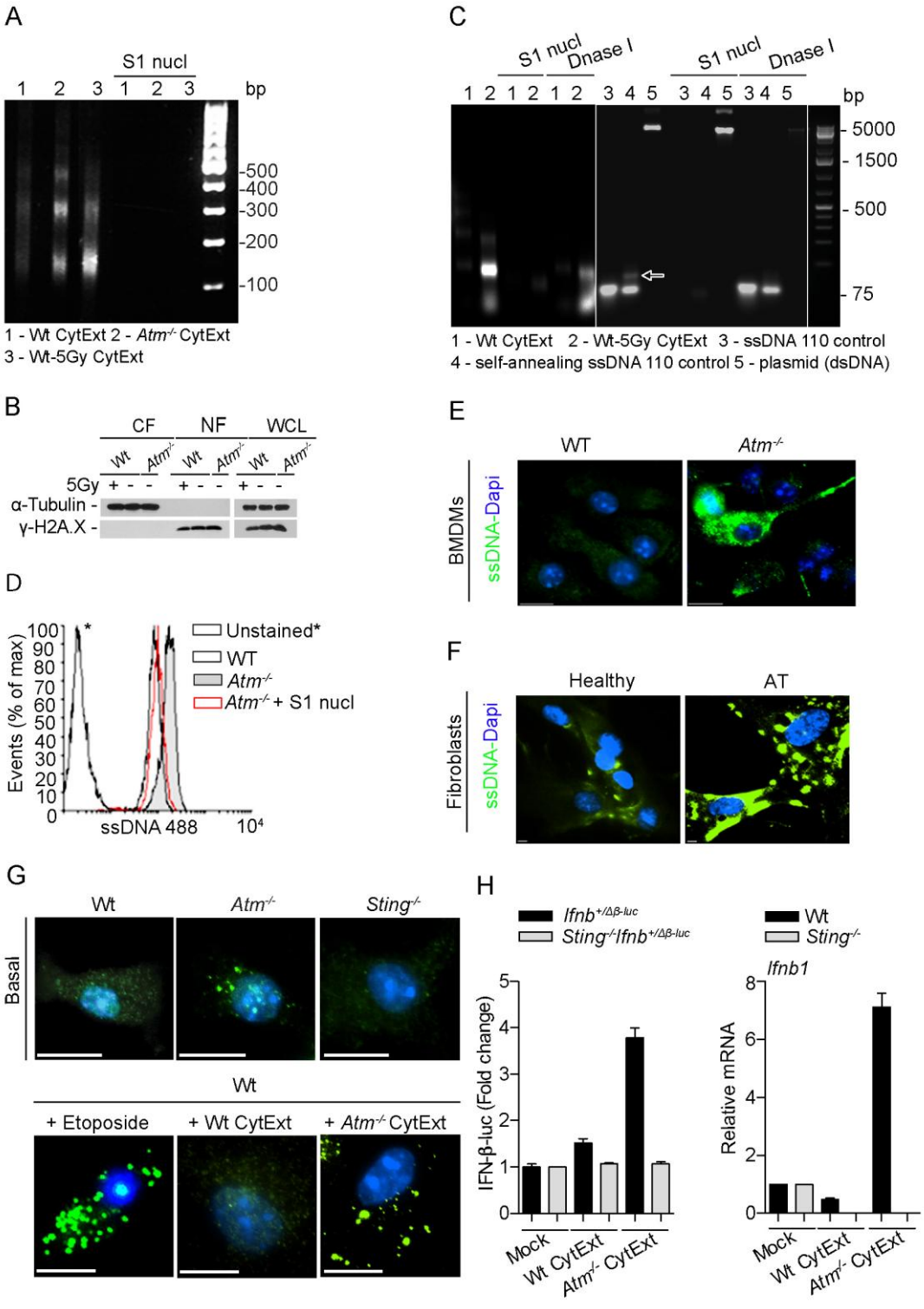


**Figure 7. DNA damage or loss of ATM results in accumulation of DNA in the cytoplasm thus activating the STING pathway. (A)** Agarose gel analysis of cytoplasmic extracts (CytExt) from Wt BMDMs (Wt CytExt), *Atm*$^{-/-}$ BMDMs (*Atm*$^{-/-}$ CytExt) at steady state or 3 hours after γ-irradiation (5Gy) of Wt BMDMs (Wt/5Gy CytExt). CytExt were treated (or not) with S1 nuclease. (**B**) Purity of sub-cellular fractions as determined by immunoblotting for γ-H2A.X and α-Tubulin in cytoplasmic fractions (CF) depicted in **A** and corresponding nuclear fraction (NF) and whole cell lysates (WCL). (**C**) Agarose gel analysis of Wt/5Gy

CytExt, ssDNA controls ssDNA 110, self-annealing ssDNA 110 or plasmid DNA treated (or not) with S1 nuclease (5 U/ml), DNase I (0.01 U/ml). White arrow in panel C indicates the self-annealed dsDNA of self-annealing ssDNA 110. (**D**) Flow cytometry analysis of methanol fixed Wt, *Atm*$^{-/-}$ BMDMs treated (or not) with S1-nuclease then stained with anti-ssDNA AlexaFluor 488. (**E** and **F)** Immunofluoresence microscopic analysis of ssDNA (green) in Wt and *Atm*$^{-/-}$ BMDMs (**E**) or fibroblasts from healthy and AT patients (**F**). (**G**) STING staining in Wt, *Atm*$^{-/-}$, *Sting*$^{-/-}$ BMDMs at steady state or in Wt BMDMs treated with etoposide for 18 hours or transfected with Wt CytExt or *Atm*$^{-/-}$ CytExt. STING was stained using anti-STING/Alexa Fluor488 conjugated secondary antibody (green) and DAPI (blue) for nuclei. (**H)** Wt CytExt and *Atm*$^{-/-}$ CytExt were transfected into *Ifnb*$^{+/\Delta\beta\text{-}luc}$ or *Sting*$^{-/-}$*Ifnb*$^{+/\Delta\beta\text{-}luc}$ macrophages and IFN-β induction was determined by luciferase assay and qRT-PCR. Data are representative of three independent experiments. Quantitative measurements are shown as mean ± SEM. Also see **Figures S5-S7**.

## Supplemental Figures

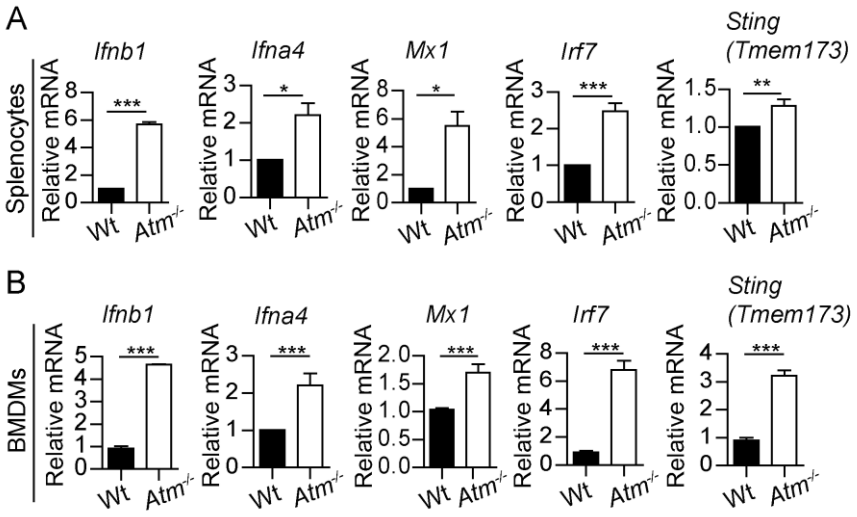


**Figure S1, related to Figure 2. Loss of ATM results in elevated spontaneous type I IFN response in mice.** (**A** and **B**) qRT-PCR analysis of *Ifnb1, Ifna4, Mx1, Irf7* and *Sting* mRNA in splenocytes (**A**) or BMDMs (**B**) from Wt or *Atm*$^{-/-}$ mice at steady state. Results are representative of three independent experiments. Data are shown as mean ± SEM. *P< 0.05, **P< 0.01, ***P< 0.001 (Student's *t*-test).

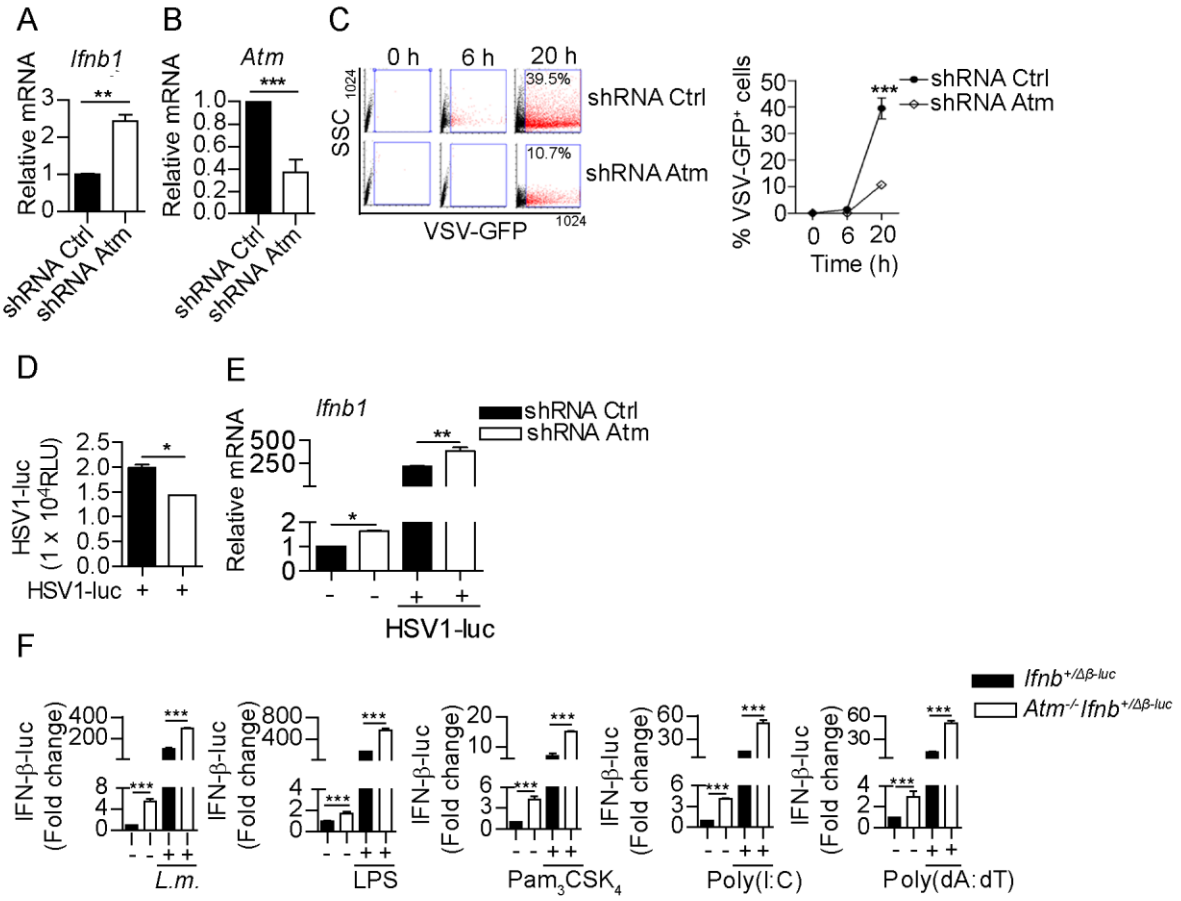


**Figure S2**, **related to Figure 2. Ablation of ATM results in increased anti-viral innate immunity.** (**A** and **B**) qRT-PCR analysis of transcripts for *Ifnb1* (**A**) and *Atm* (**B**) in RAW 264.7 macrophages transduced with lentivirus with shRNA Ctrl (control) or shRNA Atm. (**C**) Flow cytometric analysis of viral load in RAW 264.7 macrophages transduced with shRNA Ctrl or shRNA Atm and infected with VSV-GFP for the indicated time points. Graph depicts quantification of VSV-GFP positive cells in FACS dot plots. (**D**) Luciferase based estimation of HSV1-luc replication and (**E**) qRT-PCR analysis of *Ifnb1* mRNA in shRNA Ctrl or shRNA Atm RAW 264.7 macrophages 6 hours post infection (or not). (**F**) Luciferase activity of IFN-β response in *Ifnb*$^{+/\Delta\beta\text{-luc}}$ and *Atm*$^{-/-}$*Ifnb*$^{+/\Delta\beta\text{-luc}}$ BMDMs infected (or not) with *L.m.* (MOI 20) or stimulated (or not) with LPS (500 ng/ml), $Pam_3CSK_4$ (200 ng/ml), Poly-(I:C) (30 µg/ml) or transfected with Poly (dA:dT) (1 µg/ml) for 6 hours. Results are representative of two to three independent experiments. Data are shown as mean ± SEM. **P< 0.01, ***P< 0.001; (Student's *t*-test).

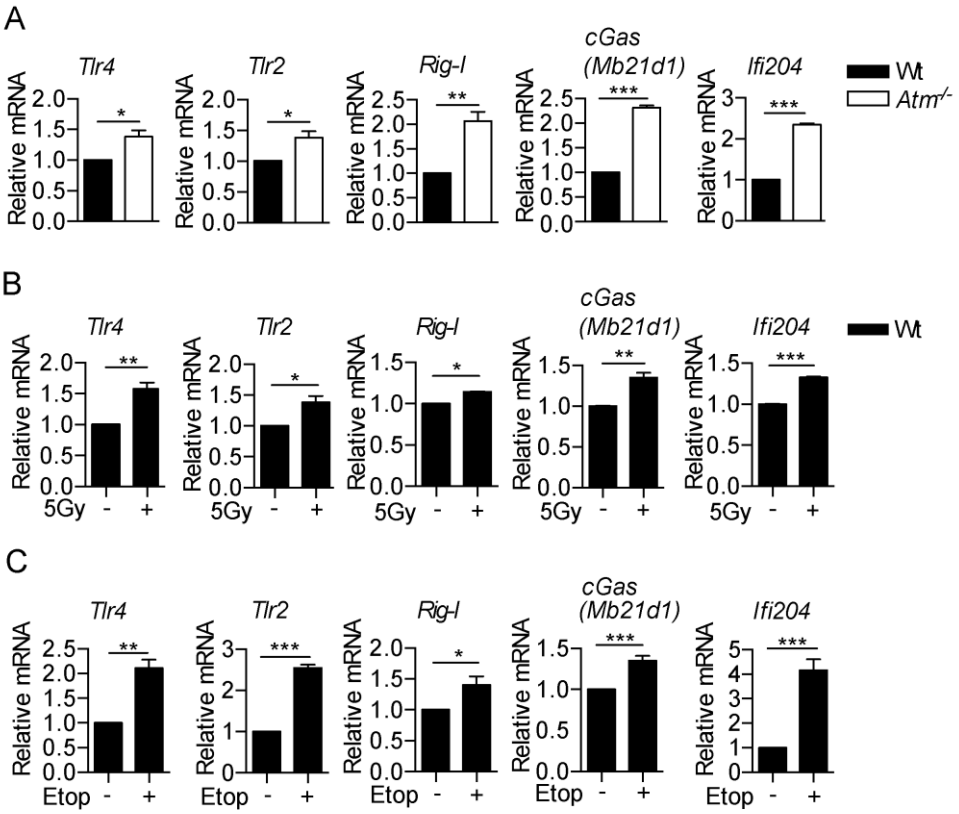


**Figure S3, related to Figure 4. Elevated expression of inflammatory genes and PRRs upon DNA damage or loss of ATM.** (**A-C**) qRT-PCR analysis of *Tlr4, Tlr2, Rig-I, cGas* and *Ifi204* mRNA in Wt and *Atm*$^{-/-}$ BMDMs at steady state (**A**), in Wt BMDMs 6 hours after γ-irradiation (5Gy) (or not) (**B**) or treated (or not) with 50 μM etoposide for 18 hours (**C**). Data are shown as mean ± SEM. *P< 0.05, **P< 0.01, ***P< 0.001; (Student's *t*-test).

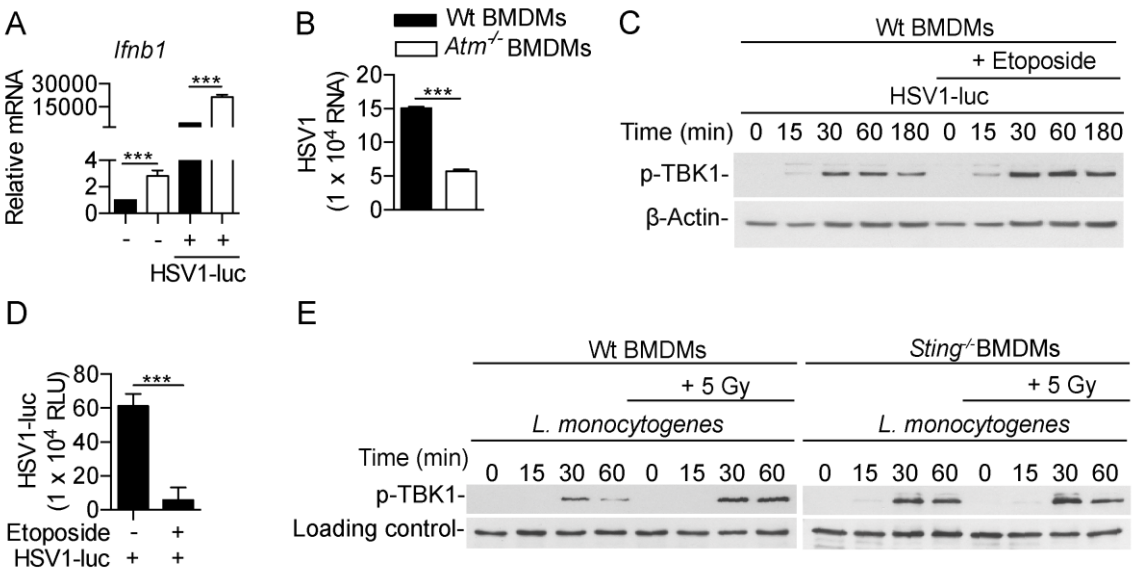


**Figure S4, related to Figure 5. Loss of ATM or exposure to DNA damage promotes anti-viral and anti-bacterial innate immunity. (A, B)** Wt or *Atm*$^{-/-}$ BMDMs infected (or not) with HSV1-luc (MOI 0.1) and analyzed by qRT-PCR after 6 hours for *Ifnb1* mRNA (**A**) or for HSV1 RNA after 12 hours (**B**). (**C**) Wt BMDM treated (or not) with etoposide (50 μM) for 18 hours, then infected with HSV1-luc (MOI 1) for indicated time points then analyzed for TBK1 phosphorylation. (**D**) RAW 264.7 macrophages treated (or not) with etoposide and infected with HSV1-luc as in C for 12 hours then analyzed for HSV1 replication by luciferase assay RLU (relative light units). (**E**) Wt and *Sting*$^{-/-}$ BMDMs primed (or not) by γ-irradiation (5Gy) and infected 3 hours later with *L.m.* (MOI 20) for the indicated durations then analyzed for TBK1 phosphorylation.

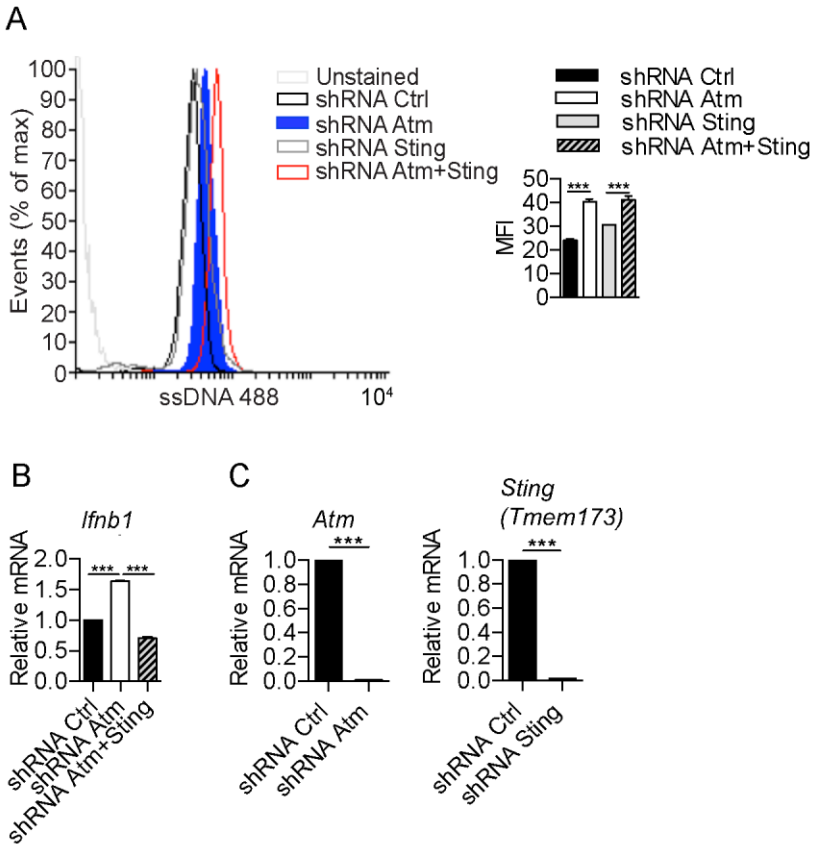


**Figure S5, related to Figure 7**. **Ablation of STING abolishes elevated type I IFN response in *Atm* silenced cells but not release of DNA into the cytoplasm**. (**A**) Flow cytometric estimation of ssDNA levels in RAW 264.7 macrophages silenced by shRNA for *Atm* (shRNA Atm), *Sting* (shRNA Sting) or both (shRNA Atm + Sting). Graph depicts corresponding Mean Fluorescence Intensitiy (MFI) of ssDNA stainings. (**B**) qRT-PCR analysis of *Ifnb1* mRNA level at steady state in indicated RAW 264.7 macrophages knockdown cell lines. (**C**) Efficiency of *Atm* and *Sting* knockdown. Results are representative of three independent experiments. Data are shown as mean ± SEM. ***P< 0.001; (one-way ANOVA followed by Bonferroni's post-test or Student's *t*-test).

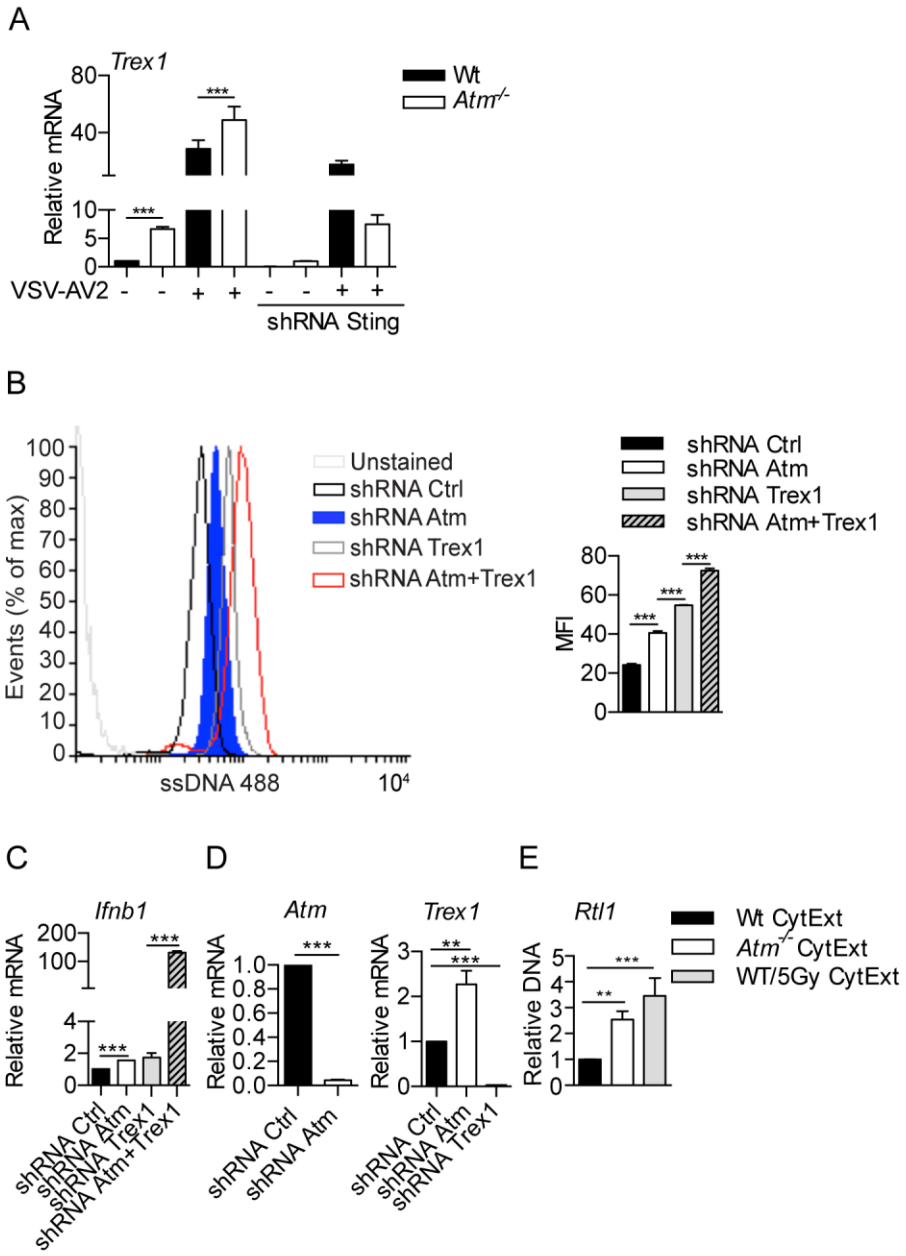


**Figure S6, related to Figure 7**. **Ablation of TREX1 augments accumulation of ssDNA in the cytoplasm and accentuates type I IFN response resulting from loss of ATM. (A)** qRT-PCR analysis of *Trex1* mRNA in WT and *Atm*$^{-/-}$ BMDMs that were silenced (or not) with shRNA Sting then infected (or not) with VSV-AV2 (MOI 1) for 6 hours. **(B)** Flow cytometric estimation of ssDNA level in RAW 264.7 macrophages silenced with shRNA for *Atm* (shRNA Atm), *Trex1* (shRNA Trex1) or both (shRNA Atm + Trex1). Graph depicts corresponding Mean Fluorescence Intensity (MFI) of ssDNA stainings. (**C**) qRT-PCR analysis of *Ifnb1* mRNA level at steady state in indicated shRNA silenced RAW 264.7 macrophages. (**D**) qRT-PCR analysis of *Atm* and *Trex1* in control or shRNA knockdown RAW 264.7 macrophages used in **B** and **C**. (**E**) qPCR analysis of retrotransposon-like 1 (Rtl1) in Wt CytExt, *Atm*$^{-/-}$ CytExt, Wt/5Gy CytExt. Results are representative of three independent experiments. Data are shown as mean ± SEM. **P< 0.01, ***P< 0.001; (one-way ANOVA followed by Bonferroni's post-test or Student's *t*-test).

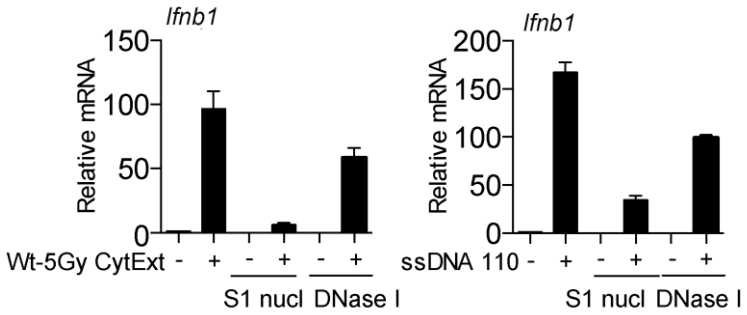


**Figure S7, related to Figure 7**. **Type I IFN stimulatory activities of CytExt DNA are sensitive to S1 nuclease and DNase I.** qRT-PCR analysis of *Ifnb1* mRNA in Wt BMDMs transfected with Wt/5Gy CytExt or ssDNA 110 pre-treated (or not) with S1 nuclease (5 U/ml) and/or DNase I (0.01 U/ml). Results are representative of two independent experiments.

# Supplemental Experimental Procedures

## Mice

*Atm*$^{-/-}$ (B6.129S6-*Atm*$^{tm1Awb}$/J) (Barlow et al., 1996), *Sting*$^{-/-}$(C57BL/6J-Tmem173gt/J) (Sauer et al., 2011) and *Ticam1*$^{-/-}$(C57BL/6J-Ticam1Lps2/J) (Hoebe et al., 2003) were from Jackson Laboratory. *Ifnb*$^{+/\Delta\beta\text{-luc}}$ (Lienenklaus et al., 2009) and *Ifnar1*$^{-/-}$ mice were provided by S. Weiss. *Myd88*$^{-/-}$(Adachi et al., 1998), *Ips-1*$^{-/-}$(Kumar et al., 2006) were from S. Akira´s laboratory. Above mice were crossed with each other at the Umeå Transgene Core Facility (UTCF) to generate the following mouse lines: *Atm*$^{-/-}$*Ifnb*$^{+/\Delta\beta\text{-luc}}$, *Atm*$^{-/-}$*Ifnar1*$^{-/-}$, *Myd88*$^{-/-}$ *Ifnb*$^{+/\Delta\beta\text{-luc}}$, *Ticam1*$^{-/-}$*Ifnb*$^{+/\Delta\beta\text{-luc}}$, *Sting*$^{-/-}$*Ifnb*$^{+/\Delta\beta\text{-luc}}$, *Atm*$^{-/-}$*Sting*$^{-/-}$*Ifnb*$^{+/\Delta\beta\text{-luc}}$, *Myd88*$^{-/-}$*Ticam1*$^{-/-}$ */Ips-1*$^{-/-}$ and *Atm*$^{+/-}$*Myd88*$^{-/-}$*Ticam1*$^{-/--}$*Ips-1*$^{-/-}$.

## Luciferase assay

Cells were lysed in 30 µl lysis buffer containing 0,2 % (v/v) Triton-X-100, 10 % (v/v) glycerol in phosphate-buffered saline (PBS). 25 µl of each lysate was mixed with 50 µl of Luciferase Assay Reagent (Promega) and measured for luciferase activity using TECAN Infinite M1000 PRO multi-mode microplate reader. Relative luminescence units were normalized to protein concentration and expressed as fold-change in relation to unstimulated wild-type values.

## Reagents and antibodies

Lipopolysaccharide (LPS), gentamicin, etoposide, mouse anti-α-Tubulin antibody, shRNAs against mouse *Atm*, *Trex1*, *cGAS*, *Ifi204*, human *IFNAR1* were from Sigma-Aldrich. $Pam_3CSK_4$, c-di-GMP, Poly (I:C), Poly (dA:dT) and Lyovec (transfection reagent) were from Invivogen. S1 nuclease was from Invitrogen. Dnase I was from Thermo Scientific. Rabbit anti-TBK1 and rabbit anti-p-TBK1 antibodies were obtained from Abcam. Mouse anti-ssDNA antibody was from Merck- Millipore. Goat anti-γ-H2A.X, rabbit anti-p-γ-H2A.X

and mouse anti-β-Actin were from Santa Cruz Biotechnology. Rabbit anti-STING was from Imgenex, anti-p-p38 MAPK and anti-p-IRF-3 were from Cell Signaling Technology. Alexa Fluor488 anti-mouse IgM and anti-rabbit IgG were from Invitrogen (Molecular Probes). Horse radish peroxidase (HRP)-conjugated anti-mouse and anti-rabbit were from Thermo Scientific. HRP conjugated anti-goat was from Santa Cruz Biotechnology. ECL Western Blotting Detection Kit (ThermoScientific), X-ray films were from Kodak.

**Plaque Assays**

Vero cells grown to 90 % confluence in six-well plates were inoculated with 10-fold serial dilutions of supernatants from infected cells in DMEM supplemented with 2 % (v/v) FCS and 20 mM HEPES (pH 7.3). After 1 h of incubation at 37°C, the inoculum was removed and cells were overlaid with 3 ml of DMEM containing 2 % (v/v) FCS, 0.02 % (w/v) DEAE-dextran, and 0.4 % (w/v) Agar Noble (Difco) and further incubated for 72 h at 37 °C. Cells were fixed and stained with 1 % (w/v) crystal violet, 3.6 % (w/v) formaldehyde, 1 % (v/v) methanol, and 20 % (v/v) ethanol, and titers were calculated from the plaque numbers and the dilution factor.

**Lentiviral shRNA gene silencing and retroviral mediated ectopic gene expression**

Lentiviruses for shRNA were produced by co-transfecting (calcium phosphate) HEK293T cells with pooled (4-5) shRNAs (Sigma-Aldrich) together with packaging plasmids pCMV-dR8.2 dvpr and pHCMV-EcoEnv (Sena-Esteves et al., 2004) (Addgene plasmids 8455 and 15802 respectively). pLKO.1 shRNA vector with unknown target in the mouse genome was used as control. Supernatants harvested after 36, 48 and 72 hours post-transfection were pooled, cleared of cell debris by centrifugation and virus particles were pelleted by ultracentrifugation at 76000 x g for 4 hours using SW28 rotor. Virus particles were resuspended in Optimem medium and either frozen down in aliquots or applied directly on to target cells in the presence of 4 μg/ml polybrene followed by centrifugation at 700 x g for 1 hour at RT. Thereafter, cells were washed twice with

PBS, lysed and harvested in 72 hours or subjected to antibiotics selection 48 hours post-transduction to establish stable lines.

**Quantitative Real-time PCR analysis**

RNA was isolated from cells using RNeasy kit from Qiagen. 1 μg of total RNA was reverse transcribed using oligo(dT) primers (New England Biolabs). Quantitative Real-time PCR analysis was performed and analyzed using ABI Prism 7500 Fast RT-PCR System (Applied Biosystems). The results were normalized to the housekeeping genes and expressed as fold change relative to RNA samples from control or mock-treated cells/mice using the comparative CT method ($\Delta\Delta_{CT}$). All Taqman gene expression data are presented as the expression relative to *18S rRNA* reference gene (RN18S1). The following TaqMan Gene Expression Assays were used (Applied Biosystems): Ifnb1 (Mm00439552_s1), Ifnα4 (Mm00833969_s1), Mx1 (Mm00487796_m1), Rn18S1 (Mm03928990_g1), Ifnb1 (Hs01077958_s1), Ifnα4 (Hs01681284_sH**),** Mx1 (Hs00895608_m1**)** and Rn18S1 (Hs03928985_g1). Viral RNAs for VSV and HSV1 were quantified by Taqman probe for VSV and HSV1. Fw=Forward, Rv=Reverse.

| Primer Name | Sequence 5'-3' |
|---|---|
| VSV Fw | 5'-gatagtaccggaggattgacgacta-3' |
| VSV Rv | 5'-tcaaaccatccgagccattc-3' |
| VSV Probe | [6FAM]tgcaccgccacaaggcagaga[BHQ1] |
| HSV1 Fw | 5'-tgggacacatgccttcttgg-3' |
| HSV1 Rv | 5'-acccttagtcagactctgttacttaccc-3' |
| HSV1 Probe | [6FAM]cgtctggaccaaccgccacacaggt[BHQ1] |

Other mRNAs were quantified by Sybr Green qPCR. The gene expression using Sybr Green qPCR were either normalized to β-Actin or ribosomal protein large, P0 (Rplp0) using validated QuantiTect primer assays (Qiagen). The following specific gene primers were used:

| Primer Name | Sequence 5'-3' |
|---|---|
| Atm (mouse) Fw | 5'-ccaggggaagatgatgaag-3' |
| Atm (mouse) Rv | 5'-gaaatcgtgcgtgacatcaaa -3' |
| β-Actin (mouse) Fw | 5'-gaaatcgtgcgtgacatcaaa -3' |
| β-Actin (mouse) Rv | 5'-tgtagtttcatggatgccaca-3' |
| cGAS (mouse) Fw | 5'-gaggcgcggaaagtcgtaa -3' |
| cGAS (mouse) Rv | 5'-ttgtccggttccttcctgga-3' |
| IFN-λ1 ( (human IFNL1) Fw | 5′-cgccttggaagagtcactca-3′ |
| IFN-λ1 (human IFNL1) Rv | 5′-gaagcctcaggtcccaattc-3′ |
| IFNAR1 (human) Fw | 5′-aacaggagcgatgagtctgtc-3′ |
| IFNAR1 (human) Rv | 5′-tgcgaaatggtgtaaatgagtca-3′ |
| Irf7 (mouse) Fw | 5′-cctcttgcttcaggttctgc-3′ |
| Irf7 (mouse) Rv | 5′-ggagcctgtggtgggac-3′ |
| P204 (mouse) Fw | 5′-tggtcccaaacaagtgatggtgc-3′ |
| P204 (mouse) Rv | 5′-tcagtttcagtagccacggtagca-3′ |
| Rig-I (mouse) Fw | 5′-ctttgcagtccctgtttggag-3′ |
| Rig-I (mouse) Rv | 5'-tgcggcagctctaaagttttc-3′ |
| Sting (mouse) Fw | 5'-aaataactgccgcctcattg-3′ |
| Sting (mouse) Rv | 5'-acagtacggagggaggagg-3′ |
| Tlr2 (mouse) Fw | 5'-gcaaacgctgttctgctcag-3′ |
| Tlr2 (mouse) Rv | 5'-aggcgtctccctctattgtatt-3′ |
| Tlr4 (mouse) Fw | 5'-agctcctgaccttggtcttg-3′ |
| Tlr4 (mouse) Rv | 5'-cgcaggggaactcaatgagg-3′ |
| Trex1 (mouse) Fw | 5'-cgtcaacgcttcgatgaca-3′ |

| | |
|---|---|
| Trex1 (mouse) Rv | 5'-agtcatagcggtcaccgtt-3′ |
| Retroelements (Retrotransposon-like 1 (Rtl1) Fw | 5′-gctatgattcaaacccggagtt-3′ |
| Retroelements (Retrotransposon-like 1 (Rtl1) Rv | 5′-ccatgctataatcggatgcctc-3′ |

The following oligonucleotides were used as controls for ssDNA: ssDNA 110 (5´-ctgcagcctgaatatgggccaaacaggatatctgtggtaagcagttcctgccccggctcagggccaagaacagatggaacagctgaatatgggccaaacaggatatctgt-3´), Self annealing ssDNA 110 (5´-ctgcagcctgaatatgggccaaacaggatatctgtggtaagcagttcctgccccgTcggggcaggaactgcttaccacagatatcctatttggcccatattcaggctgcag-3´)